STUDY OF THE MAGNETIC AND TRANSPORT PROPERTIES OF YTTERBIUM DOPED Co-Zn FERRITES

M.Sc. Thesis

BY

MD. DELOAR HOSSAIN

DEPARTMENT OF PHYSICS
KHULNA UNIVERSITY OF ENGINEERING & TECHNOLOGY
KHULNA - 9203, BANGLADESH

OCTOBER- 2018

STUDY OF THE MAGNETIC AND TRANSPORT PROPERTIES OF YTTERBIUM DOPED Co-Zn FERRITES

M.Sc. Thesis

BY

MD. DELOAR HOSSAIN
ROLL NO. 1755506
SESSION: JANUARY-2017

A THESIS SUBMITED TO THE DEPARTMENT OF PHYSICS, KHULNA UNIVERSITY OF ENGINEERING & TECHNOLOGY, KHULNA - 9203 IN PARTIAL FULFILMENT OF THE REQUIRMENT FOR THE DEGREE OF MASTER OF SCIENCE

DEPARTMENT OF PHYSICS
KHULNA UNIVERSITY OF ENGINEERING & TECHNOLOGY
KHULNA - 9203, BANGLADESH

OCTOBER- 2018

KHULNA UNIVERSITY OF ENGINEERING & TECHNOLOGY
DEPARTMENT OF PHYSICS

Approval

This is to certify that the thesis submitted by ***Md. Deloar Hossain*** entitled ***"Study of the Magnetic and Transport Properties of Ytterbium Doped Co-Zn Ferrites"*** has been accepted by the Board of Examiners for the partial fulfillment of the requirements for the degree of M. Sc. in the Department of Physics, Khulna University of Engineering & Technology, Khulna, Bangladesh on 22 October 2018.

Board of Examiners

Sl. No. **Name, Designation & Address**

1. Prof. Dr. Shibendra Shekher Sikder
   Department of Physics
   Khulna University of Engineering & Technology
   ..... Chairman & Supervisor

2. Head
   Department of Physics
   Khulna University of Engineering & Technology
   ..... Member

3. Prof. Dr. Md. Mahbub Alam
   Department of Physics
   Khulna University of Engineering & Technology
   ..... Member

4. Prof. Dr. Md. Abdullah Elias Akhter
   Department of Physics
   Khulna University of Engineering & Technology
   ..... Member

5. Prof. Dr. Farid Ahmed
   Department of Physics
   Jahangirnagar University, Savar, Dhaka
   ..... Member (External)

DECLARATION

This is to certify that the thesis work entitled as **"Study of the Magnetic and Transport Properties of Ytterbium Doped Co-Zn Ferrites"** has been carried out in partial fulfillment of the requirement for M.Sc. degree in the Department of Physics, Khulna University of Engineering & Technology, Khulna-9203, Bangladesh. The above research work or any part of this work has not been submitted to anywhere for the award of any degree or diploma. No other person's work has been used without due acknowledgement.

Supervisor

.....

Prof. Dr. Shibendra Shekher Sikder

Candidate

.....

Md. Deloar Hossain

TO

MY PARENTS

Acknowledgements

First of all I express all my admiration and devotion to the almighty Allah, the most beneficent who has enabled me to perform this research work and to submit this thesis

I would like to express my deep sense of gratitude and high gratefulness with due respect to my Supervisor Professor Dr. Shibendra Shekher Sikder, Department of Physics, Khulna University of Engineering & Technology (KUET), Khulna for considering me as a thesis student. His guidance, enthusiastic concern, positive and regular inspiration and constructive supervision made the work easy and successful.

I am indebted to Professor Dr. Md. Mahbub Alam, Head, Department of Physics, KUET, for his co-operation and inspiration during this work. I also grateful to Professor Dr. Md. Abdullah Elias Akhter, Department of Physics, KUET, who always liked to give me mental support that was so essential for me during the time of research.

I want to give my warm and deep gratitude to Dr. A. K. M. Abdul Hakim, Individual Consultant & Guest Faculty, Department of Glass & Ceramic Engineering (GCE), Bangladesh University of Engineering & Technology (BUET), who always think about research, new ideas and try to guide young researchers which made them passionate about research. His valuable direction, suggestions and continuous assessment on work made me conscious and sincere to obtain better results in all experiments.

I am grateful to Dr. S. Manjura Hoque, Head & Chief Scientific Officer, and Dr. Mohammed Nazrul Islam Khan, Principal Scientific Officer (PSO), Materials Science Division (MSD), Atomic Energy Centre, Dhaka (AECD) for providing kind opportunity to use the laboratory for experimental work.

I would like to express my special gratitude and thanks to Md. Alamgir Hossain and Mr. Sujit Kumar Shil, Assistant Professor, Department of Physics, KUET, for their support, suggestions and provisions that benefited me much in the completion of this thesis work.

I gratefully acknowledge Professor Dr. Joly Sultana, Department of Physics, KUET. My thanks are also for Md. Kamrul Hasan Reza, Associate Professor,

Mr.Suman Halder, and Mr. Suman Debnath, Assistant Professor, Mr. Probal Roy, Md. Saifullah, Md. Idris Ali, Sazzad Hossain, Lecturer, Department of Physics, KUET, for their moral support.

I am highly indebted and thoroughly grateful to Md. Ali Reza for his great suggestion and effort from the very beginning of this research work. It was really hard for me to be a research student in KUET without his suggestion and motivation. Special thanks to Md. Rabiul Hossain, Al-Masud and Md. Noman Hossain, KUET for providing their kind help throughout this work.

I am very glad to acknowledge the support from my well-wishers Md. Nazmul Hossain (BUET), Subroto Subon Acharjee, Prodip Kumar Mondal, Kaushik Sarkar, Kamrun Nahar and Sharmin Akhter, Solid State Physics Lab, KUET.

I would like to give thanks from deep of my heart to my parents Md. Mozammel Haque and Most. Asia Begum, my younger brother Md. Romzan Ali, my elder brother Md. Mahedi Hasan, my room-mate Abdullah Al Aman, and specially Md. Milon Islam, Lecturer, Department of CSE, KUET for their comprehensive mental support and love. I have not much word to express my gratefulness to them.

My thanks are due to Director, Atomic Energy Centre, Dhaka for his kind permission to use the Laboratory of Materials Science Division, Atomic Energy Centre, Dhaka.

I also wise to thank the authority of Khulna University of Engineering & Technology (KUET), for providing me with the necessary permission and financial assistance for conducting this thesis work.

Md. Deloar Hossain

ABSTRACT

The present research work is focused Ytterbium (Yb) doped Co-Zn ferrites. The ferrite samples of the composition $Co_{0.25}Zn_{0.75}Yb_xFe_{2-x}O_4$ [where x = 0.00, 0.02, 0.04, 0.06 and 0.08] were prepared by standard solid state reaction technique. The samples were pre-sintered at 850°C for 2 hours and sintered at 1150°C for 3 hours. The effect of rare earth Yb^{3+} substitution on the structural, magnetic and electrical properties of the Co-Zn ferrites was studied. The Phase identification and lattice parameter determination were carried out by using X-ray diffraction (XRD). XRD patterns showed that all the samples consisted of the singe phase cubic spinel structure with no extra peak**.** The lattice parameters gradually increased with increasing Yb content. The bulk density slightly decreased with increasing rare earth Yb^{3+} ion and the X-ray density increased continuously with increasing x-content. The microstructural analysis was done by Scanning Electron Microscopy (SEM). The SEM images showed that the sample exhibit uniform surface morphology with well-defined spherical grains. The average grain size was calculated using Image J software and observed that the average grain size increases with Yb content. The complex permeability, loss tangent and dielectric properties were investigated as a function of frequency range 1 KHz to 120 MHz by using an impedance analyzer. The initial permeability was found in steady state to a higher order of frequency range from 10^3Hz - 50 MHz. Continuous decrease of the dielectric constant with the increasing frequency and remains almost constant at higher frequency range has been observed. The magnetic properties have been studied by Vibrating Sample Magnetometer (VSM). The saturation magnetization (M_s), coercivity (H_c), remanent magnetization (M_r), Bhor magneton (μ_B), and anisotropy constant (K_u) have been calculated from the M-H loop at room temperature. The values of M_s were decreased with increasing Yb^{3+} content. Coercivity was increased with Yb content except for X = 0.08 where it decreased. The values of μ_B were found to be decreased with increasing Yb^{3+}content. Doping of Yb ion lowers the conduction and subsequently an increase in resistivity is observed. The characteristics of electromagnetism, excellent chemical stability, mechanical hardness, high coercivity, and moderate saturation magnetization have made Yb doped Co-Zn ferrite a good candidate for synthesizing and investigation to contribute in science and technology.

Contents

CHAPTER-III

EXPERIMENTAL PROCEDURE

CHAPTER-IV

RESULTS AND DISCUSSION

CHAPTER-V

CONCLUSIONS

List of Figures

List of Tables

List of Symbols

XRD	=	X-Ray Diffraction
VSM	=	Vibrating Sample Magnetometer
SEM	=	Scanning Electron Microscopy
DC	=	Direct Current
RE	=	Rare Earth
FCC	=	Face Centered Cubic
T_N	=	Nell Temperature
ρ_B	=	Bulk density
ρ_x	=	X-ray density
ρ_{DC}	=	DC Resistivity
M_S	=	Saturation magnetization
M_r	=	Remanent magnetization
K_u	=	Anisotropy constant
H_c	=	Coercive force
μ_B	=	Magnetic moment in Bohr magneton.
μ	=	Permeability
μ'	=	Real part of the complex permeability
μ''	=	imaginary part of the complex permeability
ε	=	Dielectric constant
ε'	=	Real part of the dielectric constant
ε''	=	imaginary part of the complex permeability
D	=	Grain size
Φ	=	Magnetic Flux
I	=	Intensity of Magnetization
B	=	Magnetic induction
H	=	Magnetic field
a	=	Lattice parameter
tan δ	=	loss factor or loss tangent
λ	=	Wave length of the X-ray

[hkl]	=	Miller Indices of a peak
δ	=	Phase Angle
R	=	Resistance
T	=	Torque
B	=	External Magnetic Field
I	=	Intensity of Magnetization
χ	=	Magnetic Susceptibility
C	=	Capacitance of a Capacitor
C_o	=	Capacitance of a Capacitor with Vacuum
$F(\theta)$	=	Nelson Riley Function
Q	=	Quality Factor
RQF	=	Relative Quality Factor

CHAPTER I

INTRODUCTION

INTRODUCTION

1.1 Introduction

Rare earth doped ferrites are very essential in today's modern technology. Small amount of rare earth substituted in the spinel ferrites are found to display interesting properties such as physical, electrical and magnetic properties. The magnetic properties of spinel ferrites are strongly dependent on microstructure refinement agent. The rare earth oxides are recently becoming the promising and potential additives for the improvement of the properties of ferrites. Rare earth elements are very large magnetostriction at low temperatures due to their localized nature of 4f electrons being totally screened by 5s and 5p orbital. Magnetism originates from the spin of unpaired electrons. Cations in ferrite lattice are separated by oxygen anions. Oxygen anions have no magnetic moment but it has completely filled shells. With p-type outer most orbits Co^{2+} (d^7), Zn^{2+} (d^{10}) and Fe^{3+} (d^5) cations of the ferrite have 3, 0 and 5 unpaired electrons respectively. So divalent Co and trivalent Fe have magnetic moments due to unfilled 3d sub shell. Zn^{2+} by contrast, is diamagnetic because the outer shell of its completely filled. The magnetic properties of the ferrites can be modified by distribution of cations in 'A' and 'B' sites through substitution. The Co-Zn ferrite is inverse spinel where half of the Fe^{3+} are in 'A' sites; remaining half and Co is 'B' sites. When Zn is substituted for Co, Zn preferentially enters into the 'A' sites by displacing a proportionate number of Fe^{3+} from 'A' to 'B' sites with a cation distribution.

Ferrites have attracted a considerable interest to the researchers due to their wide range of scientific and technological applications in electronics, optoelectronics, magnetic, magneto-electronics, electrochemical science and technology, and biotechnology [Rahman *et at.,* 2014; Razia *et at.,* 2012; Sajjia *et at.,* 2014; Shirsath *et at.,* 2012]. Ferrites are electrically non-conductive ferrimagnetic ceramic compound materials, consisting of various mixtures of iron oxides such as Hematite (Fe_2O_3) or Magnetite (Fe_3O_4) and the oxides of other metals like NiO, CuO, ZnO, MnO, CoO. According to their crystal structure spinel type ferrites are natural super lattices and they have tetrahedral A-site and octahedral B-site in AB_2O_4 crystal structure. This material shows various magnetic properties depending on the cation distribution of the chemical compositions. Various cations can be placed in A-site and B-site to tune

their magnetic properties. Depending on A-site and B-site cations, they can exhibit ferrimagnetic, antiferromagnetic, spin(cluster) glass and paramagnetic behavior [Akther Hossain *et at.,* 2008]. Moreover, ferrite materials are insulating magnetic oxides and possess high electrical resistivity, low eddy current and dielectric losses, high saturation magnetization, high permeability and moderate permittivity. No material with such wide ranging properties exists and therefore ferrites are unique magnetic materials which find applications in almost all fields.

Co-Zn ferrites are soft spinel cubic remain the best magnetic materials and cannot be replaced by any other magnetic materials with respect to their very high frequency application because they are inexpensive, more stable, easily manufactured etc. They have wide range of technological applications in transformer core, inductors, high quality filters, radiofrequency circuits, rod antennas, read/ write heads for high speed digital tape and operating devices [Nakamura *et at.,* 2003; Laksman *et at.,* 2002]. Every item of electronic equipment produced today contains some ferromagnetic spinel ferrite materials. The several compositions of such ferrites is MFe_2O_4, where M is the divalent transition metals such as Mn, Zn, Ni, Co, Cu, Fe or Mg etc. Many researchers have worked on different types of ferrites in order to improve their electrical and magnetic properties such as Ni-Zn [Hossain *et at.,* 2017], Ni-Cu-Zn [Khan *et at.,* 2013], Mg-Zn [Abbas *et at.,* 2015] ferrites.

Among various ferrites, polycrystalline Co-Zn ferrite could be considered as the most versatile ferrites, due to their several advantages over others ferrites such as low cost of raw materials, low density, and high operating frequency. Co-Zn ferrite is one of the soft ferrites used in electronic and magnetic devices such as transformers, inductors and magnetic heads for high frequency because their electrical resistivity is higher than those of the soft magnetic alloys. Co-Zn ferrites which are the mixture of $CoFe_2O_4$ and $ZnFe_2O_4$ ferrites. Now the mixture of $ZnFe_2O_4$ and $CoFe_2O_4$ have been most extensively studied systems, because they exhibit the typically normal and inverse spinel ferrites respectively [Sathishkumar *et at.,* 2010, Saroaut Noor *et. al.* 2012]. Zinc ferrite bulk is antiferromagnetic below the Neel temperature (T_N = 10K) and turns to ferromagnetic or super paramagnetic when particle size reduces. In $ZnFe_2O_4$, zinc ions occupy the tetrahedral sites and all Fe^{3+} ions occupy the octahedral sites. In contrast, $CoFe_2O_4$ exhibits ferromagnetism where cobalt ions occupy the octahedral sites and Fe^{3+} ions are equally distributed in tetrahedral and octahedral sites. Therefore, Co-Zn mixed ferrite has attracted considerable attention due to the

completely different and interesting properties of $ZnFe_2O_4$ and $CoFe_2O_4$. Dilute $CoZnFe_2O_4$ with nonmagnetic Zn content higher than percolation limit where frustration and competing interaction start to play dominant role has hitherto not been studied in much detail except a detail study carries out by $Co_{0.25}Zn_{0.75}Fe_2O_4$ with substitution of Ytterbium (Yb). The composition $Co_{0.25}Zn_{0.75}Fe_2O_4$ is chosen because this diluted composition is expected to show complex magnetic structures that consists of long range ferromagnetic ordering, antiferromagnetic ordering and clustering effects. In this present research, a composition of ferrite is prepared to investigate the effect of (Yb^{3+}) in the $Co_{0.25}Zn_{0.75}Yb_xFe_{2-x}O_4$ ferrite by solid state reaction technique. There are several issues related to the rare earth Yb doping in ferrites such as limited solubility of Yb ions and its effect on the electrical and magnetic properties which are not well understood. Therefore, in this study, an attempt is being made to investigate in detail the effects of substitution of (Yb^{3+}) ions on the structural, electrical and magnetic properties of $Co_{0.25}Zn_{0.75}Yb_xFe_{2-x}O_4$ ferrites and also to enhance these properties for further industrial applications.

1.2 The Aims and Objectives of the Present Work

Ferrites are especially convenient for high frequency uses because of their high resistivity. The high frequency response of the complex permeability is therefore very useful in determining the convenient frequency range in which a particular ferrite material can be used. The small amount of rare earth ions to Co-Zn ferrites samples produces a change in their magnetic and transport properties as well as structural and electrical properties of rare element like Yb used. The main purpose of this work Cu-Zn ferrites of composition $Co_{0.25}Zn_{0.75}Yb_xFe_{2-x}O_4$ [Where x = 0.00, 0.02, 0.04, 0.06 and 0.08] and hence to study the effect of substitution of rare earth Ytterbium ions (Yb^{3+}) doped on the surface morphology, saturation magnetization, initial permeability, complex permeability, magnetic loss, quality factor and transport properties like dielectric constant and electric resistivity. The effect of composition and microstructure on the frequency response is therefore very useful.

The main objectives of the present research are as follows:

- Preparation of various $Co_{0.25}Zn_{0.75}Yb_xFe_{2-x}O_4$ [Where x = 0.00, 0.02, 0.04, 0.06 and 0.08] samples by solid state reaction technique.

- Determination of crystal structure (X-ray diffraction), density and porosity of Co-Zn ferrite.
- Optimize the concentration of Yb to partially replace Fe in Co-Zn ferrite for the best magnetic and transport properties. To study structural, electrical, transport and magnetic properties of all the prepared samples such as microstructure, magnetization, magnetic loss components, permeability, resistivity, dielectric constant etc.

Finally, it is expected to use powder particles as starting materials may give uniform microstructure exhibiting better magnetic and electrical transport properties. The complex permeability, magnetization, electrical properties are also expected to change due to the incorporation of Yb^{3+}. Thus this system will have further good technological application in high frequency range. In our research in soft magnetic materials and in rare earth metal doped ferrites, Bangladesh may develop a profitable electronic industry.

1.3 Experimental Reason for this Research Work

Rare earth metal doped ferrites sample have been prepared by standard solid state reaction technique. High purity powders of Co_3O_4 (99.9%), ZnO (99.9%), Yb_2O_3 (99.9%), Fe_2O_3 (99.9%) has been mixed thoroughly in an appropriate amount mixing will be performed in both dry and acetone. The mixed powder has been calcined at high temperature. After calcinations toroid and disk shaped sample has been prepared and will be sintered at various temperatures. The experimental methods that have been used in this work are as follows:

(i) The prepared sample would be characterized in terms of their crystal structure, unit cell parameters and phase presents in the prepared sample with the help of X-ray diffraction (XRD) in the Material Science Division, Atomic Energy Center (AEC), Dhaka.

(ii) Sintering of the samples has been carried out in a microprocessor controlled high temperature furnace in the Department of Physics, KUET, Khulna.

(iii) Surface morphology of the samples has been investigated using scanning electron microscope (SEM) in the Material Science Division, Atomic Energy Center (AEC), Dhaka.

(iv) Permeability, magnetic loss factor and quality factor as function of frequency have been determining using impedance analyzer in the Department of Physics, KUET, Khulna.

(v) Magnetizations of the samples have been measured as a function of field using vibrating sample magnetometer (VSM) in the Material Science Division, Atomic Energy Center (AEC), Dhaka.

(vi) Dielectric properties as a function of frequency have been studied with the help of inductance meter in the Department of Physics, KUET, Khulna.

(vii) DC electrical resistivity as a function of Yb content has been studied with help of electrometer in the Department of Physics, KUET, Khulna.

The incorporation of rare earth metal ion Yb^{3+} doping Co-Zn ferrite will be affects the surface morphology by modifying the lattice parameters and grain size. The magnetic properties like magnetization, initial permeability, quality factor and transport properties like dielectric constant, electrical resistivity of Co-Zn ferrites are also expected to change due the incorporation of Yb^{3+} ion. Overall, the quality of the prepared samples Co-Zn-Yb ferrites has been interpreted on the basis of existing theories of magnetic materials than the mother alloy Co-Zn ferrites.

1.4 Ferrites and their Importance

The outstanding property of ferrite which first attracted the attention was their negligible electrical eddy current losses that make in ferrites indispensable materials in telecommunications and in the electronic industry. Saturation magnetization (M_S), coercive force (H_C) and initial permeability (μ_i) are the most important parameters for the good quality presentation in application and secret by the initial permeability, for the low and high frequency applications. Ferrites are used widely due to their following application.

- **Inductors and transformers:** Ferrites are one of the core materials used in inductors and transformers. They are widely used as inductive components in a huge variety of electronic circuits as in low noise amplifiers, filters, voltage-controlled oscillators, impedance matching networks.
- **High Frequency applications:** Ferrites are using extensively for high-frequency applications such as in telecommunications and radar systems, as microwave technology requires higher frequencies and bandwidths up to 100 GHz. Ferrites are non-conducting oxides and consequently tolerate total

penetration of electromagnetic fields, in contrast with metals, where the skin effect strictly limits the penetration of high-frequency fields.

- **Ferrites for modern devices:** Ferrites are largely used in radio engineering and television circuits, antennae, video cassette recorders (VCR's), picture tube deflection Yokes, fly back transformers, audio and intermediated frequency transformers and SMPS transformer for power applications, memory devices, digital systems, tapes, audio and video recording heads, electronic devices which are operated from low to high frequency range.
- **Ferrites for Electromagnetic Interference Suppression:** The major increment in the quantity of electronic equipments such as digital circuits in broad band amplifiers, communication systems, power controls, digital cameras, scanners, computer equipment, control processors, weapons systems, life support and other medical systems and so forth, in small areas, has hazardously improved the option of disturbing each other by electromagnetic interference (EMI).
- **High-density write-once optical recording:** Thin films of defect spinel ferrites may be used as write-once read-many media functioning through blue wavelengths. In fact, since these non-stoichiometric ferrites are metastable, they can be distorted into corundum phases at moderate temperatures by a laser spot. The distorted regions have diverse optical indices from the starting ferrite film, making the readout procedure probable.
- **Magnetic shielding:** A radar absorbing paint containing ferrite has been developed to render an aircraft of submarine invisible to radar.
- **Magnetic sensors:** Magnetic sensors are used for temperature control and can be made by using ferrite material with sharp and definite Curie temperature. Position and rotational angle sensors (proximity switches) have also been designed using ferrites.
- **Pollution control:** There are several Japanese installations which use precipitation of ferrite precursors for searching pollutant materials such as mercury from waste streams. The ferrites formed subsequently can be alienated magnetically along with the pollutant.

- **Ferrite as electrodes*:*** As ferrites have high corrosion resistance, therefore, having the appropriate conductivities they can be used as electrode in applications mainly in chromium plating.

1.5 Background of Material Selection: Literature Review

In recent years, rare earth substituted different ferrites are becoming promising materials for various applications. Addition of small amount of rare earth ions to ferrite sample alters their electrical, magnetic and structural properties depending upon the type and amount of rare earth element used [Nikumbhet *et at.,* 2014; Song *et at.,* 2010; *et at.,* 2014]. Rare earth ions can be divided into two categories; one with the radius closes to Fe ions; while other with ionic radius larger than Fe ions [Rezlescu *et at.,* 1994]. The difference in their ionic radii will lead to micro strains which may cause domain wall motion resulting in deformation of the spinel structure [Jacob *et at.,* 2011]. It has been stated that the rare earth ions commonly reside at the octahedral sites by replacing Fe^{3+}ions and have limited solubility in the spinel lattice due to their large ionic radii. If the rare earth ions enter the spinel lattice the RE-Fe interaction also appears (4f-3d coupling) which can lead to changes in the magnetization and Curie temperature. The rare earth oxides are good electrical insulators and have resistivity at room temperature greater than 10^6 Ω-cm [Ahmed *et at.,* 2017]. Rare earth ion forms the orthoferrite phase.

Pandya *et at.,* (1991) investigated a spinel ferrite system $Zn_xCo_{1-x}Fe_2O_4$ that was prepared by a wet chemical method before and after high temperature annealing. Here the low field a.c. susceptibility measurements indicate that the low temperature synthesis of wet prepared Co–Zn ferrites aids the formation of spin-clusters and thereby increases the magnetic properties. On the other hand X-ray analysis confirmed that the sample was spinel ferrite.

Nalla Somaiah *et at.,* (2012) investigated that Cobalt-Zinc ferrite based materials are suitable candidates for magneto mechanical sensor applications. X-ray spectra analysis and transmission electron microscopy studies revealed that the as-prepared powders were comprised of cubic-spinel phase with irregularly shaped grains morphology. The peak value of magnetostriction decreases with increasing Zn content. They also observed that the Zn-doped Cobalt ferrite (x = 0.1) having high strain derivative could be a potential material for stress sensor application.

Anshu *et at.,* (2012) reported that $Co_xZn_{1-x}Fe_2O_4$ (x = 0, 0.02, 0.04, and 0.06) showed cubic spinel structure with minor Fe_2O_3 phase and lattice parameter decreases with increasing cobalt content. Magnetic measurement showed that Co-Zn ferrite exhibit ferromagnetic behavior at room temperature.

Slatineanua *et at.,* (2013) investigated Magnetic and dielectric properties of Co–Zn ferrite with the chemical formula $Co_xZn_{1-x}Fe_2O_4$ (x = 0, 0.2, 0.4, 0.6, 0.8, 1). Magnetic behavior of the as-obtained samples by means of M-H hysteresis measurements was studied at room temperature. In agreement with the proposed cation distribution the sample with $Co_{0.8}Zn_{0.2}Fe_2O_4$ formula exhibits the optimal magnetic and dielectric behavior. Lopez *et at.,* 2012 recently synthesized Zn doped CoFe2O4 magnetic nanoparticles by using a co-precipitation method. They observed decrease in coercive field and particle size with the increase of Zn concentration.

Gul *et at.,* (2007) investigated magnetic and electrical properties of $Co_{1-x}Zn_xFe_2O_4$ varying x from (0.0 to 0.6). A decrease in Curie temperature with an increasing Zinc doping concentration was observed. Temperature dependent dc resistivity measurements indicated semiconductor nature in Co-Zn ferrites.

Veverka *et at.,* (2011) studied $Co_{1-x}Zn_xFe_2O_4$ around x = 0.6. They reported that the cationic distribution in ferrite is more complex and the distribution is random in nature. They also observed that presence of vacancies in the octahedral sites changed the cobalt ions partially or completely to the Co^{3+} state. A neutron diffraction study showed the differences of cationic distributions in nanoparticles and bulk ferrite samples.

The structural and magnetic properties of Co-Zn ferrite films with high saturation magnetization have been synthesized by Urcia *et at.,* (2010). They observed the X-ray diffraction, transmission electron microscopy, and Raman spectroscopy analyses suggested both the actual incorporation of the dopants into the host ferrite lattice and the promoting effect on crystal size of the flow rate at which the reactants are contacted. The strong dependence of the magnetic properties of cobalt-zinc mixed ferrite with specific dopant species enables this material to be considered a promising candidate for magnetocaloric applications.

The effect of substitution Fe^{3+} ions by rare earth Nd^{3+} ions on structure, magnetic properties of cobalt ferrite nanocrystals was investigated by Lijun Zhao *et at.,*(2006). The saturation magnetization for rare earth Nd^{3+}doped samples was less than that of pure cobalt ferrite. On the other hand, the value of coercivity is increased

with the Nd^{3+}doped content. The pure cobalt ferrite powders with crystallite sizes of 10.3 nm achieved values of M_S = 53.4 emu/g and H_C = 172.0 Oe.

The RE (RE = La, Ce, Pr, Nd, Sm, Eu, Gd, Tb, and Dy) and Mn ions co-doped Co–Zn ferrites were synthesized by Ying Zhang, Dijiang Wen (2012). They reported that The substitution leads to non-monotonous change of the lattice parameters and infrared emissivity properties, which is mainly attributed to the partial cation exchange among the spinel structure of Co–Zn ferrites. The infrared emission properties of Co–Zn ferrites seem to be greatly influenced by the co-doped of RE^{3+} and Mn ions maxima values were 0.96–0.97, found for LaF, NdF and GdF, respectively.

Shivaji *et at.,* (2012) studied the rare earth Dysprosium doped Co–Zn ferrites, synthesized by sol–gel auto combustion method. They observed that the average grain size increases with increasing the Dy content in the Co–Zn ferrite.The XRD study of Dy doped Co–Zn ferrite shows in Cubic spinel phase. Particle size obtained from TEM analysis was found to be 30–40 nm.

Ji-Jing *et at.,* (2009) reported the impact of the rare earth La^{3+} substitution improved of magnetization (σ_s) and decrease of coercivity (H_c) of Co-Zn ferrites. The increase of the substitution ratio of La^{3+} ions from 0.0 to 0.3, the lattice parameters a and c increased gradually, which resulted in the change of the particle shape and size. The rare earth La^{3+} ions doped in the ferrite not only improved complex permeability and complex permittivity, but also microwave absorbency.

Kambale *et at.,* (2011) investigated the effect of Dy^{3+} substitution on the structural and magnetic properties of $CoFe_{2-x}Dy_xO_4$ (x = 0.00 to 0.1 in step of 0.025) system. They found the microstructural features were observed by SEM that demonstrates the fine clustered particles with an increase of average grain size with Dy^{3+} content. Room temperature magnetization measurements showed that the saturation magnetization and hysteresis losses (coercivity) decreases with Dy^{3+} addition.

Karimi *et at.,* (2014) studied the structural and magnetic perspective of rare earth Dy^{3+} doped cobalt ferrites with the chemical formula $Co_{1-x}Dy_xFe_2O_4$ (x = 0, 0.01, 0.03, 0.05, 0.1). The spinel phase formation was confirmed via x-ray diffractometry, and the other crystallographic parameters. The hysteresis loop of the material was affected noticeably by doped elements as the room temperature

saturation magnetization was decreased, but the residual magnetization and coercivity of ferrite were promoted by 50 and 150% after adding dysprosium, respectively.

From the above discussion we can say that, spinel ferrites are very important for academic and technological applications. In this research, the proposed sample has the formula of $Co_{0.25}Zn_{0.75}Yb_xFe_{2-x}O_4$ [where x = 0.00, 0.02, 0.04, 0.06, 0.08]. Now the reason of Co-Zn ferrite selection has been attributed by studying common problems with Co-Zn ferrites.

1.6 Outline of the Thesis

The thesis has been configured into five chapters which are as follows:

Chapter 1: Introduction

This chapter presents a brief introduction to Co-Zn ferrites with composition $Co_{0.25}Zn_{0.75}Yb_xFe_{2-x}O_4$ and organization of thesis. This chapter incorporates background information to assist in understanding the aims and objectives of this investigation, and also reviews recent reports by other investigators with which these results can compared.

Chapter II: Theoretical Background

In this chapter, a briefly describe theories necessary to understand magnetic materials as well as ferrites, classification of ferrites, fundamental quantities of magnetism, theory of initial permeability, dielectric constant etc. have been discussed in details.

Chapter III: Experimental Background

In this chapter, the experiment procedures are briefly explained along with description of the sample preparation, raw materials. This chapter deals with mainly the design and construction of experimental and preparation of ferrite samples. The fundamentals and working principles of measurement set up are discussed.

Chapter IV: Results and Discussion

In this chapter, results and discussion are thoroughly explained. The various experimental and theoretical studies namely Study of the Magnetic and Transport Properties of Ytterbium Doped Co-Zn Ferrites are presented and discussed step by step.

Chapter V: Conclusion

This chapter represents an overview of the results as obtained from all previous chapters. Few suggestions towards the future scope have also been discussed.

References are added at the end of this chapter.

CHAPTER II

THEROETICAL BACKGROUND

THEROETICAL BACKGROUND

2.1 Overview of Rare Earth Ferrites

Rare earth elements are a set of seventeen chemical elements in the periodic table, specifically the fifteen lanthanides, as well as Scandium (Sc) and Yttrium (Y). The fifteen lanthanide elements are Lanthanum (La), Cerium (Ce), Praseodymium (Pr), Neodymium (Nd), Promethium (Pm), Samarium (Sm), Europium (Eu), Gadolinium (Gd), Terbium (Tb), Dysprosium (Dy), Holmium (Ho), Erbium (Er), Thulium (Tm), Ytterbium (Yb), and Lutetium (Lu). Scandium is found in most rare earth element deposits and is sometimes classified as a rare earth element. The International Union of Pure and Applied Chemistry include scandium in their rare earth element definition. The rare earth substituted different ferrites are becoming the promising materials for different applications. Addition of small amount of rare earth ions to ferrite samples producing a change in their magnetic and electrical as well as structural properties depending upon the types and the amount of rare earth elements used.

Rare earth metals are actually not as rare as their name might imply. They are simply more difficult to mine than most metals and generally don't accumulate into rich ores. This rarity, combined with the demand for the metals in high-tech applications, brings about economic and political complications that make some of the most interesting metals even more exciting. The rare earth elements are all metals, and the group is often referred to as the "rare earth metals". These metals have many similar properties and that often causes them to be found together in geologic deposits. They are also referred to as "rare earth oxides" because many of them are typically sold as oxide compounds. Rare earth elements are not as "rare" as their name implies. Thulium and lutetium are the two least abundant rare earth elements - but they each have an average crustal abundance that is nearly 200 times greater than the crustal abundance of gold [Rare Earth Elements]. However, these metals are very difficult to mine because it is unusual to find them in concentrations high enough for economical extraction.

The better properties of ferrites can be achieved through proper doping of rare earth metals and recently rare earth (RE) doped ferrites become interesting due to their superiority for various applications such as structural, magnetic and electrical

properties over other doped ferrite systems[Bharathi *et al.,* 2009; Peng *et al.,* 2011; Guo *et al.,* 2010; Nikumbh *et al.,* 2014].

Doping the parent spinel ferrite with rare earth ions leads tostructural disorder and lattice strain, thereby increasing the electrical and magnetic parameters [Jacobo *et al.,* 2004 and Shil *et. al.,* 2012]. The difference in their ionic radii will lead to micro strains, which may cause domain wall motion resulting in deformation of the spinel structure. The rare earth ions have unpaired 4f electrons and the strong spin orbit coupling of the angular momentum. Moreover, 4f shell of rare earth ions is shielded by $5S^2 5P^6$ and almost not affected by the potential field of surrounding ions. Doping rare earth ions into spinel type ferrites, the occurrence of 4f-3d couplings which determine the magneto-crystalline anisotropy in spinel ferrite can also improve the electric and magnetic properties of spinel ferrites [Jing *et al.,* 2006; Jing *et al.,* 2007; Vanuitert 1955; Kolekar *et al.,* 1995]. Spinel ferrites ceramic are widely used in microwave devices to control transmission path, frequency, amplitude and phase of microwave signals. Accurate dielectric and magnetic properties measurement at the operational frequency and temperature ranges are needed for optimized development of these devices, as well as to assist in the manufacture of the ferrite [Jie *et al.,* 2010]. The structured magnetic materials have an interesting area of study because of its possible applications in a variety of widely areas ranging from information technology to biotechnology [Bahadur *et al.,* 2005]. The properties of ferrites are being improved due to the increasing trends in ferrite technology. It is believed that there is a bright future for ferrite technology. Ferrimagnetisms in ferrite is largely governed by Fe-Fe interaction, i.e. the spin coupling of the 3d electron. In view of the great interest of rare earth doped Co-Zn ferrites, both their technological applications and theoretical understanding of the mechanisms involved, the present work is aimed at finding the effect Yb ions. A large number of workers are engaged in research to bring about improvement on the qualities of rare earth doped Co-Zn ferrites has been improve in all aspects than the3 mother alloy Co-Zn ferrites.

2.2 Brief History of Ferrimagnetism and Ferrites

In ferrimagnetic materials atoms have opposing magnetic moments or magnetic field strengths, but these opposing magnetic moments are unequal. Therefore, these exist some net magnetic moment. The ferrimagnetic material does not lose its magnetism even in the absence of external magnetic field.

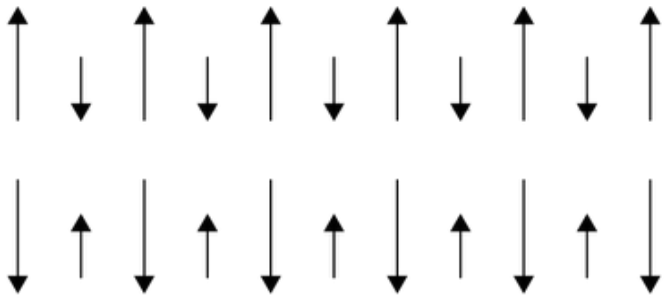

Figure 2.1: Magnetic Moments in Ferrimagnet.

In ionic compounds, such as oxides, more complex forms of magnetic ordering can occur as a result of the crystal structure. One type of magnetic ordering is call ferrimagnetism. A simple representation of the magnetic spins in a ferrimagnetic oxide is shown here. The magnetic structure is composed of two magnetic sublattices (called A and B) separated by oxygen's. The exchange interactions are mediated by the oxygen anions. When this happens, the interactions are called indirect or super exchange interactions. The strongest super exchange interactions result in an antiparallel alignment of spins between the A and B sublattice the magnetic moments of the A and B sublattices are not equal and result in a net magnetic moment. Ferrimagnetism is therefore similar to ferromagnetism. It exhibits all the hallmarks of ferromagnetic behavior- spontaneous magnetization, Curie temperatures, hysteresis, and remanence.

Ferrites are electrically non-conductive ferrimagnetic ceramic compound materials, consisting of various mixtures of iron oxides such as Hematite (Fe_2O_3) or Magnetite (Fe_3O_4) and the oxides of other metals like NiO, CuO, ZnO, MnO, CoO. They are both electrically nonconductive and ferrimagnetic, meaning they can be magnetized or attracted to a magnet. On the other hand ferrites are a class of ferrimagnetic ceramic chemical compounds consisting of mixtures of various metal oxides, usually including iron oxides. Their general chemical formula may be written as AB_2O_4, where A and B represent different metal cations. These ceramic materials are used in applications ranging from magnetic components in microelectronics.

At high frequencies ferrites are considered superior to other magnetic materials because they have low eddy current losses and high DC electrical resistivity. The DC electrical resistivity of ferrites at room temperature can vary deep-ending upon the chemical composition.

2.3 Types of Ferrites

According to crystallographic structures ferrites can be classified into three different types [Standley, 1972]

(i) Spinel ferrites (Cubic ferrites)

(ii) Hexagonal ferrites

(iii) Garnets

Our research work is on spinel ferrites; therefore we shall discuss in detail the spinel ferrites only.

2.3.1 Spinel Ferrites

They are also called cubic ferrites. Spinel is the most widely used family of ferrites. High values of electrical resistivity and low eddy current losses make them ideal for their use at microwave frequencies. The spinel structure of ferrites as possessed by mineral spinel $MgAl_2O_4$ was first determined by Bragg and Nishikawa in 1915. The chemical composition of a spinel ferrite can be written in general as MFe_2O_4 where M is a divalent metal ion such as Co^{2+}, Zn^{2+}, Fe^{2+}, Mg^{2+}, Ni^{2+}, Cd^{2+} or a combination of these ions.

The unit cell of spinel ferrites is FCC with eight formula units per unit cell. The formula can be written as $M_8Fe_{16}O_{32}$. The anions are the greatest and they form an FCC lattice. Within these lattices two types of interstitial positions occur and these are occupied by the metallic cations. There are 96 interstitial sites in the unit cell, 64 tetrahedral (A) and 32 octahedral (B) sites.

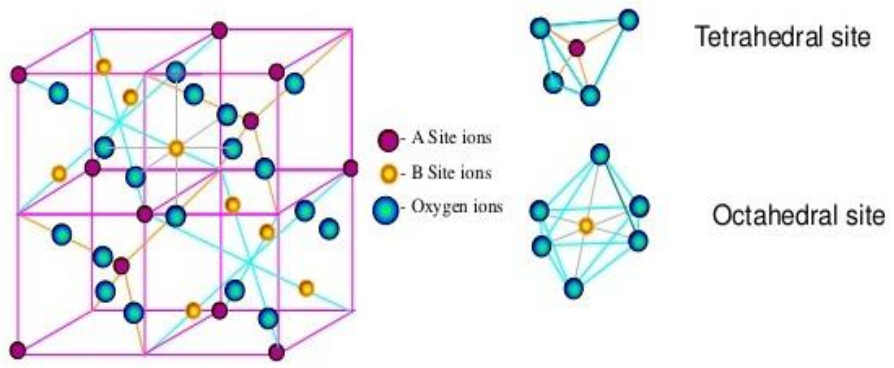

Figure 2.2: Crystal Structure of spinel ferrite

- **Tetrahedral Site**

(i) 8 A-sites metal ions in tetrahedral site coordination with oxygen,

(ii) Tetrahedral site, the interstitial is at the center of a tetrahedron formed by the four lattice atoms.

(iii) Three adjacent atoms are in a plane; the fourth atom is located at the top symmetrical position.

(iv) The tetrahedral site defined geometry provides a space for an interstitial atom

- **Octahedral Site**

(i) 16 B-sites demonstrates octahedral site

(ii) An interstitial atom at the space in the interstices between 6 atoms forming regular octahedron.

(iii) Four regular atoms are positioned in a single plane; the remaining two are located at symmetrical positions just above or below.

For a total of 56 atoms, there are 96 interstices between the anions in the cubic lattice; but in spinel ferrites, only 24 are occupied by cations. Out of the 64 tetrahedral interstices between the anions, only 8 are occupied by the cations. The rest of 16 cations occupied half of the 32 octahedral interstices. Consequently, there are 8 formula units per cubic unit cell.

Table 2.1**:** Metal ion arrangements in spinel ferrite unit cell with composition ($MO.Fe_2O_3$) [Sanpo and Noppakun]

Types of interstitial site	**Number available**	**Number occupied**	**Normal spinel**	**Inverse spinel**
Octahedral	64	8	$8M^{2+}$	$8Fe^{3+}$
Tetrahedral	32	16	$16Fe^{3+}$	$8Fe^{3+}$ $8M^{2+}$

In spinel oxide, normally the different cations do not have a big difference in size, because the spinel structure is stable only if the cations have rather medium size and in addition, the ionic radii of the different metal species in the same compound are comparable and do not differ too much. Similar cation combinations are presented in sulphides e.g. $Zn^{2+}Al_2^{3+}S_4$ and $Cu_2^{2+}Sn^{4+}S_4$.

However, in such spinels halide e.g. $Li_2^{1+}Ni^{3+}F_4$ and $Li^{1+}Mn_2^{3+/\,4+}O^4$, cations are limited to valance state of +1 and +2, in order to exhibit an overall cation: anion ratio of 3:4 The position of the "*A"* ions is almost identical to those occupied by the

carbon atoms in the diamond structure. This could explain the relatively good hardness and high density of this typical group. More than one hundred compounds of spinel structure reported to date. Most of them are oxides, some are sulphides, selenides and telluride and few are halides. A large variety of cations might be introduced into the spinel structure and different charge combinations are possible; almost any combination that has eight positive charges to balance eight anionic charges, for example, $Mg^{2+}Fe_2{}^{3+}O_4$, $Mg^{2+}Al_2{}^{3+}O_4$, $Mg_2{}^{2+}Ti^{4+}O_4$, $Li^{1+}Al^{3+}Ti^{4+}O_4$, $Li_{0.5}{}^{1+}Al_{2.5}{}^{3+}O_4$, and $Na_2{}^{1+}W^{6+}O_4$ etc.

The factors affecting the cation distribution over A- and B-sites are as follows [Alex Goldman, 1990; Craik, 1975]:

- Ionic size of cations
- Electromagnetic configuration of the cations
- Electronic energy

Smaller cations prefer to occupy the A-sites. The cations have special preference for A and B-sites and the preference depend upon the following factors:

- Ionic radius
- Size of interstices
- Temperature
- Orbital preference for the specific coordination

The preference of cations is according to Verwey-Heilman scheme given in the Table 2.2 [Verway *et al.,* 1947]:

Table: 2.2: Site preferences of metallic ions

Ions having a preference for A-sites	**Ions having a preference for B-sites**	**Ions having no specific site preference**
Zn^{2+}	Ni^{2+}	Mg^{2+}
Cd^{2+}	Cr^{3+}	Mn^{2}
Ga^{2+}	Ti^{4+}	Cu^{2+}
In^{3+}	Sn^{4+}	Fe^{2+}
Ge^{4+}		Fe^{3+}
Li^{+}		Al^{3+}

2.3.2 Hexagonal Ferrites

Hexaferrites are hexagonal or rhombohedral ferromagnetic oxides with formula $MFe_{12}O_{19}$, where M is an element like Barium, Lead or Strontium. In these ferrites, oxygen ions have closed packed hexagonal crystal structure. They are widely used as permanent magnets and have high coercivity. They are used at very high frequency. Their hexagonal ferrite lattice is similar to the spinel structure with closely packed oxygen ions, but there are also metal ions at some layers with the same ionic radii as that of oxygen ions. Hexagonal ferrites have larger ions than that of garnet ferrites and are formed by the replacement of oxygen ions. Most of these larger ions are barium, strontium or lead.

2.3.3 Garnets

Garnets are usually known as minerals. In the context of magnetic materials, garnets are represented by a general formula $Y_3Fe_5O_{12}$ containing two magnetic ions, one typically being iron and another being rare earth (RE). Here RE, in addition to yttrium can be one of lanthanide atoms such as lanthanum, cerium, samarium etc. In garnet ferrites, orbital magnetic contribution of iron atoms is quenched due to shielding from crystal field while lanthanide ions contribute to both orbital and spin magnetic moment, thus contributing more to the total magnetic moment.

Garnets can be quite useful materials in microwave applications because of their high electrical resistivity and hence lower losses around microwave frequencies. The material is also easy to synthesize in either of bulk polycrystalline ceramic, single crystal or thin film forms. The structural parameters as well as magnetic properties can be tuned by tailoring the composition of the material.

2.4 Types of Ferrites

Due to the persistence of their magnetization, the ferrites are of two types i.e. hard and soft. This classification is based on their ability to be magnetized or demagnetized. Soft ferrites are easily magnetized or demagnetized whereas hard ferrites are difficult to magnetize or demagnetize [Cullity, 1972].

2.4.1 Soft Ferrites

Soft ferrites are those that can be easily magnetized or demagnetized. These are characterized by low coercive forces and high magnetic permeability's. The low

coercivity means the materials magnetization can easily reverse direction without dissipating much energy (hysteresis losses), while the materials high resistivity prevents eddy currents in the core, another source of energy loss, generally exhibit small hysteresis losses. At high frequency metallic soft magnetic materials simply cannot be used due to the eddy current losses. Therefore soft ferrite, which is ceramic insulators, becomes the most desirable material.

These materials are ferromagnetic with a cubic crystal structure and the general composition $MO.Fe_2O_3$ where M is a transition metal such as nickel, manganese, magnesium, zinc, cobalt or cadmium. The magnetically soft ferrites first came into commercial production in 1948. Additionally, parts of the family of soft ferrites are the microwave ferrites e.g. Yttrium iron garnet .These ferrite are used in the frequency range from 100 MHz to 500GHz. For waveguides, for electromagnetic radiation, and in microwave device such as phase shifters. Application of soft ferrite include: cores for electro-magnets, electric motors, transformers, generators, and other electrical equipment. Because of their comparatively low losses at high frequencies they are extremely used in the cores of RF transformers and inductors in the applications such as a switched mode power supplies.

2.4.2 Hard Ferrites

Hard ferrites are difficult to magnetized or demagnetized. Hard magnets are characterized by high remanent inductions and high coercivities. The higher coercivity means the materials are very resistant to becoming demagnetized an essential characteristic for a permanent magnet. They also conduct magnetic flux will and have a high magnetic permeability. This enables these so-called ceramic magnets to store stronger magnetic fields than iron itself. They are cheap and are widely used in household products such as refrigerator magnets. They generally exhibit large hysteresis losses. Hard ferrite referred to as permanent magnets retain their magnetism after being magnetized.

Hard ferrite likes Ba-ferrite, Sr-ferrite, Pb-ferrite are used in communication device operating with high frequency currents because of their high resistivity, negligible eddy currents and lower loss of energy due to Joule heating and hysteresis. These are found useful in many applications including fractional horse-power motors, automobiles, audio- and video-recorders, earphones, computer peripherals, and clocks.

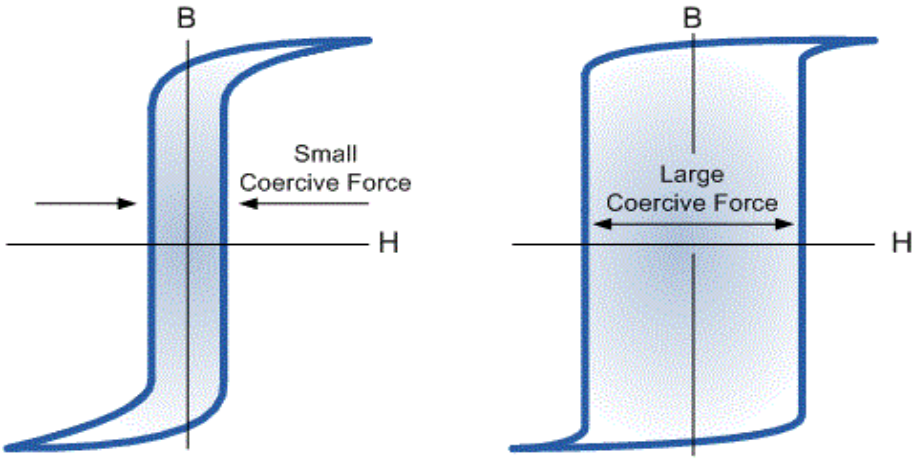

(a) (b)

Figure 2.3: (a) Soft Ferrite, (b) Hard Ferrite

2.5 Magnetism and its Origin

The word magnetism is used for those physical phenomena, which involve magnetic field and their effect upon materials. The name magnet was used by the Greeks for a stone, which was capable of attracting pieces of the same materials and iron as well. The original magnet (loadstone) is the naturally occurring magnetic iron oxide, i.e. magnetite. Some of magnetite's properties were known to humankind even before 600 B.C.

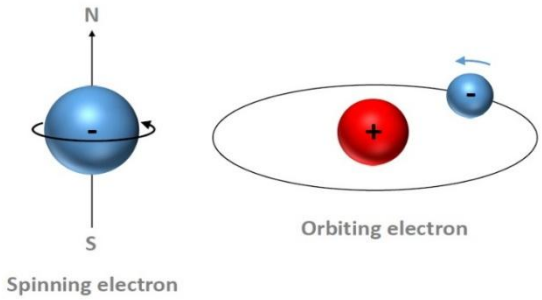

Figure 2.4: Origin of magnetism

Magnetism arises from two types of motions of electrons in atoms—one is the motion of the electrons in an orbit around the nucleus, similar to the motion of the planets in our solar system around the sun, and the other is the spin of the electrons around its axis, analogous to the rotation of Earth about its own axis. The orbital and the spin motion independently impart a magnetic moment on each electron causing each of them to behave as a tiny magnet.

Spin magnetic moment + Orbital magnetic moment = Atomic magnetic moment

2.6 Theory of Initial Permeability

Initial permeability describes the relative permeability of a material at low values of B. The maximum value for μ in a material is frequently a facing of between 2 and 5 or more above its initial value. Low flux has the advantage that every ferrite can be measured at that density without risk of saturation. This consistency means that comparison between different ferrite is easy.

For high frequency application, the desirable property of a ferrite is the high initial permeability with low loss. The present goal of the most of the recent ferrite researches is to fulfill this requirement. The initial permeability μ_i is defined as the derivative of induction B with respect to the initial field H in the demagnetization state.

$$\mu_i = \frac{dB}{dH} / H \to 0, B \to 0 \quad (2.1)$$

At microwave frequency and also in low anisotropic materials, dH and dB may be in different directions. The permeability is thus a tensor character. In the case of amorphous materials containing a large number of randomly oriented magnetic atoms the permeability will be scalar. As we have

$$B = \mu_0(H+M) \quad (2.2)$$

and susceptibility

$$\chi = \frac{dM}{dH} = \frac{d}{dxH}\left(\frac{B}{\mu_0} - 1\right) = \frac{1}{\mu_0}(\mu - 1) \quad (2.3)$$

The magnetic energy density

$$E = \frac{1}{\mu_0} \int H.dB \quad (2.4)$$

For time harmonic fields $H = H_0$ Sin wt. The dissipation can be described by a phase difference between B^+ and B.

Permeability is namely defines as the proportional constant between the magnetic field induction B and applied intensity H:

$$B = \mu H \quad (2.5)$$

If a magnetic material is subjected to an AC magnetic field as given below:

$$H = H_0 e^{i\omega t} \quad (2.7)$$

Then it is observed that the magnetic flux density B experiences a delay. The delay is caused due to presence of various losses and is thus expressed as

$$B = B_0 e^{i(\omega t - \delta} \quad (2.8)$$

Where δ is the phase angle and marks the delay of B with respect to H. The permeability is then given by

$$\mu = \frac{B}{H} = \frac{B_0 e^{i(\omega t - \delta)}}{H_0 e^{i\omega t}} = \frac{B_0 e^{-i\delta}}{H_0} = \frac{B_0}{H_0}\cos\delta - i\frac{B_0}{H_0}\sin\delta \qquad (2.9)$$

$$\mu = \mu' - i\mu'' \qquad (2.10)$$

$$\text{Where } \mu' = \frac{B_0}{H_0}\cos\delta \qquad (2.11)$$

$$\mu'' = i\frac{B_0}{H_0}\sin\delta \qquad (2.12)$$

The real Part μ' of complex permeability μ represent the component of B induction which is in phase with H, so it corresponds to the normal permeability. If there is no losses , we should have μ = μ', The imaginary part μ'' corresponds to that part of B which is delayed by phase angle δ from H arranging up to 90° from H . The presence of such a component requires a supply of energy to maintain the alternating magnetization regardless of the origin of delay.

2.7 Magnetization Process

A review of magnetization process, namely the response of ferro-or ferri magnetic material (bulk) to an applied field with a semi-microscopic approach is presented. In ferromagnetic or ferrimagnetic material, the magnetization curves, especially in low magnetic fields differ widely from sample to sample and as a function of the magnetic history of the sample i.e., of the previous fields which have been successively applied.

2.7.1 Magnetization Curve

For unmagnetized bulk materials, there is a zero net magnetic moment. It can be predicted that there will be an infinite number of degree of magnetization between the unmagnetized and saturation conditions, when the material is subjected to an external magnetic field. These extreme situations are corresponds respectively to random orientation of domains complete alignment is one direction with elimination of domain walls. If we start with a demagnetized specimen and increase the applied magnetic field, the bulk material will progressively magnetized by the domain dynamics. The magnetization of the sample will follow the course as shown in Figure 2.5 [Samokhvalov and Rustamov, 1964]. The slop from the origin to a point on the

curve r the ratio MH is defined as magnetic susceptibility. This curve is called magnetization curve. This curve is generally perceived as being made of three major portions.

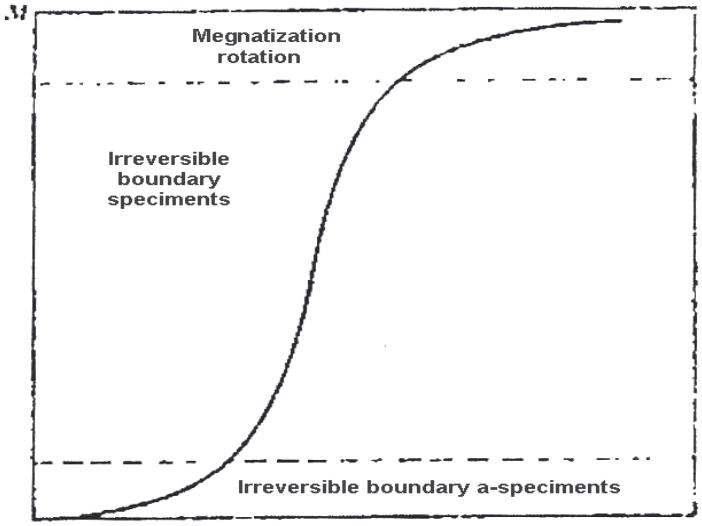

Figure 2.5: Domain dynamics during various parts of the magnetization curve

The first, the lower section, is the initial susceptibility region and characterized by reversible domain wall movements and rotations. By reversible means that after the magnetization slightly with an increase in field the origin magnetization can be reversed if the field is reduced to initial value. The condition of the displacement walls to an initial permeability is entirely dependent on the sort of material studied

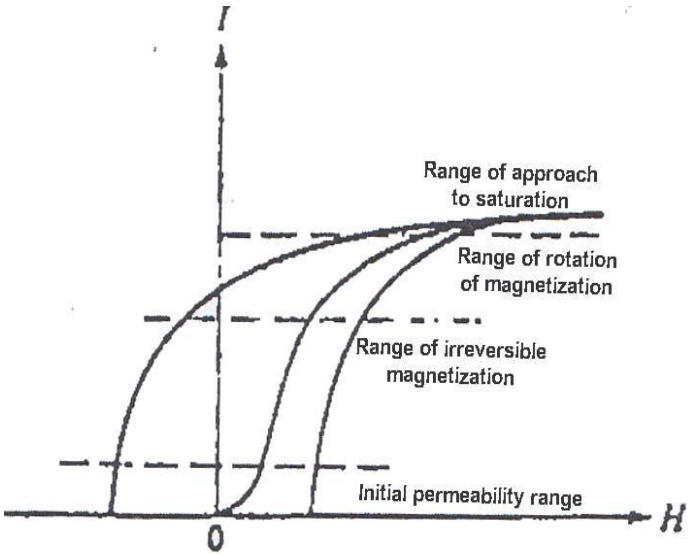

Figure 2.6: Magnetization curve and the classification of magnetization mechanism

In the second stage magnetization curve if the field is increased, the intensity of the magnetization increases more drastically is called the irreversible magnetization range. This range is obtained mainly by the reversible domain wall motion from one stable state to another If the field is increased further, the magnetization curve less step and its process become reversible once more. In the third section of magnetization curve, the displacement of domain walls have all ready been completed and the magnetizations take place by rotation magnetization. This range is called rotation magnetization range. Beyond this range the magnetization gradually approaches to saturation magnetization shown in Figure 2.6

2.8 Dielectric Constant

Dielectric constant is defined as the ratio of the capacitance of a capacitor filled with a given dielectric to the capacitance of the same capacitor with vacuum. It is a number without dimensions, a quantity measuring the ability of a substance to store electrical energy in an electrical field. If C represents the capacitance of a capacitor with dielectric and C_0 represents the capacitance of the same capacitor with vacuum, then the dielectric constant (ε') can be given by

$$\varepsilon' = \frac{C}{C_o} \qquad (2.13)$$

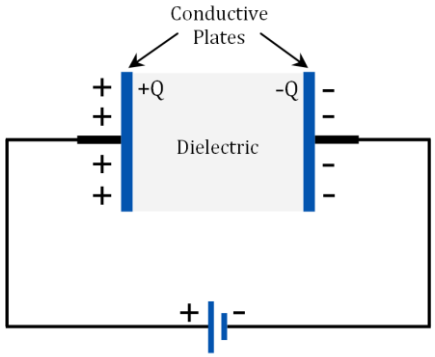

Figure 2.7: Schematic illustration of capacitive cell

But capacitance C of a parallel plate capacitor can be expressed as

$$C = \frac{\varepsilon A}{d} \qquad (2.14)$$

where, A is the area of each plate, d represents the separation between the plates and ε represents the permittivity of the dielectric material within the cpacitor.

If ε_o represents the permittivity of the free space, then from equation (2.13) we get

$$\varepsilon' = \frac{\varepsilon}{\varepsilon_o} \qquad (2.15)$$

Therefore, dielectric constant can also be defined as the ratio of the permittivity of a substance to the permittivity of free space. It is an expression of the extent to which a material concentrates electric flux, and is the electrical equivalent of relative magnetic permeability.

2.8.1 Dependence of Dielectric Constant on Frequency

Polarization systems respond to an electrical field by shifting their masses around and forms dipoles. These shifted masses are accelerated and de-accelerated with the change of the applied field which takes some time. Therefore, the polarization mechanism of a system depends on the frequency of the applied electrical field. Alternating electrical field induces alternating forces to the dipoles. Since the dipole response to a field involves the movement of masses, inertia will prevent the arbitrarily fast movements. When the frequency of the applied field increases, this movement of dipoles also increases. At high frequency, the dipoles are unable to cope with it. So at very high frequencies all movement of dipoles will 'die out' and there will be no response of the dipoles to the frequency field [Dai *et al.*, 2012]. Dielectric constant (ε') is a measure of polarization of a system, it also depends on the frequency of the applied field. In general as frequency increases, its dielectric constant drops. But for some material the dielectric constant can increase with the increase in frequency due to the parasitic effect but only at the low temperature.

2.9 DC Resistivity of Ferrites

Extensive investigation into the origin of the electrical conductivity of the spinels has been carried out by Verwey *et al.*, 1947 and Jonker, 1959. The resistivity of ferrites at room temperature can vary, depending on chemical composition between about 10^{-2} to higher than 10^{+11} ohm-cm [Valenzuela, 1994]. The low value of resistivity is due to the simultaneous presence of ferrous and ferric ions on equivalent lattice sites (octahedral). For example Fe_3O_4 at room temperature has resistivity of approximately 7×10^{-3} Ohm-cm and Fe_2O_4 with some deficiency in iron and sintered in a sufficiently oxidizing atmosphere so that the product contains no ferrous ions can have a resistivity higher than 7×10^{6} ohm-cm. To make high resistivity ferrites one must sure that there are no ferrous ions in the stoichiometric ferrites.

Temperature dependent resistivity of ferrites follows Arrhenius relation [Smit and Wijn, 1959]:

$$\rho = \rho_0 e^{\frac{E_a}{kT}}, \qquad (2.16)$$

Where ρ is the resistively and E_a is the activation energy required for hopping of an electron from one lattice site to another.

2.10 Microstructure

A polycrystal is much more than many tiny crystals bonded together. The interfaces between the crystals, or the grain boundaries which separate and bond the grains, are complex and interactive interfaces. The whole set of a given material's properties of mechanical, chemical and especially electrical and magnetic depend strongly on the nature of the microstructure. The grain boundary is the region, which accommodates the difference in crystallographic orientation between the neighboring grains. For certain simple arrangements, the grain boundary is made of an array of dislocations whose number and spacing depends on the angular deviation between the grains. The ionic nature of ferrites leads to dislocation patterns considerably more complex than in metals, since electrostatic energy accounts for a significant fraction of the total boundary energy. For low-loss ferrite, Goldman, 1999 states that the grain boundaries influence properties by

(i) creating a high resistivity intergranular layer,

(ii) acting as a sink for impurities which may act as a sintering aid and grain growth modifiers,

(iii) Providing a path for oxygen diffusion, which may modify the oxidation state of cations near the boundaries.

In addition to grain boundaries, ceramic imperfections can impede domain wall motion and thus reduce the magnetic property. Among these are pores, cracks, inclusions, second phases, as well as residual strains. Imperfections also act as energy wells that pin the domain walls and require higher activation energy to detach. They affect the domain dynamics and are responsible for a much greater share of the degradation of properties than would expect grain growth kinetics depends strongly on the impurity content. A minor do pant can drastically change the nature and concentration of defects in the matrix, affecting grain boundary motion, pore mobility and pore removal [Yan and Johnson, 1978]. The effect of a given do pant depends on its valence and solubility with respect to host material. If it is not soluble at the sintering temperature, the do pant becomes a second phase which usually segregates to the grain boundary.

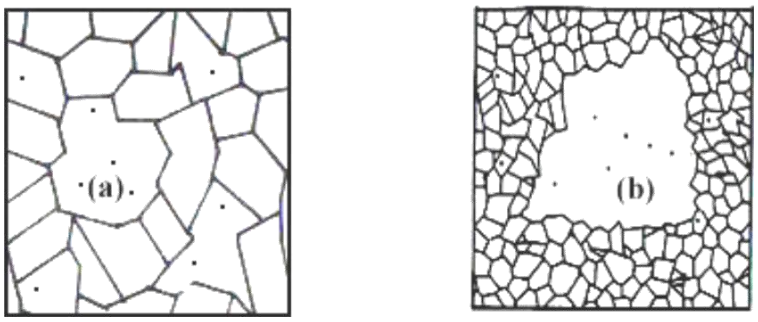

Figure 2.8: Porosity character: (a) intergranular, (b) intragranular

The porosity of ceramic samples results from two sources, intragranular porosity and intergranular porosity as shown in Figure 2.8. An undesirable effect in ceramic samples is the formation of exaggerated or discontinuous grain growth which is characterized by the excessive growth of some grains at the expense of small, neighboring ones, Figure 2.9. When this occurs, the large grain has a high defect concentration. Discontinuous growth is believed to result from one or several of the following: powder mixtures with impurities; a very large distribution of initial particle size; sintering at excessively high temperatures; in ferrites containing Zn and /or Mn, a low O^2 partial pressure in the sintering atmosphere. When a very large grain is surrounded by smaller ones, it is called ‘duplex’ microstructure.

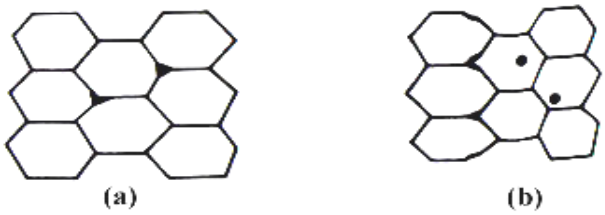

Figure 2.9: Grain growth (a) discontinuous, (b) duplex (schematic).

CHAPTER III

EXPERIMENTAL PROCEDURE

EXPERIMENTAL PROCEDURE

3.1 Rare Earth Ferrite Preparation

The preparation of rare earth ferrites with optimum desired properties is still a complex and difficult task. In this chapter, experimental methods of sample preparation techniques of rare earth Ytterbium doped Co-Zn ferrites are described briefly. We describe also the effect of the preparation, calcinations and sintering process of the rare earth substituted Co-Zn ferrites with the general formula $Co_{0.25}Zn_{0.75}Yb_xFe_{2-x}O_4$. The rare earth ferrite is not completely defined by its chemistry and crystal structure but also requires knowledge and control of parameters of its microstructure such as density grain size, porosity and their intra and intergranular distribution. In this work conventional ceramic method has been employed for the preparation of $Co_{0.25}Zn_{0.75}Yb_xFe_{2-x}O_4$ ferrites for its relative simplicity and availability.

3.2 Composition of the Studied Ferrites

In the present work the various compositions of rare earth (Yb) substituted Co-Zn ferrites are synthesized, characterized and investigated. The ferrite sample preparation facility is available in Solid State physics Lab at Khulna University of Engineering and Technology (KUET). The ferrites under investigation are:

(i) $Co_{0.25}Zn_{0.75}Fe_2O_4$

(ii) $Co_{0.25}Zn_{0.75}Yb_{0.02}Fe_{1.98}O_4$

(iii) $Co_{0.25}Zn_{0.75}Yb_{0.04}Fe_{1.96}O_4$

(iv) $Co_{0.25}Zn_{0.75}Yb_{0.06}Fe_{1.94}O_4$

(v) $Co_{0.25}Zn_{0.75}Yb_{0.08}Fe_{1.92}O_4$

3.3 Sample Preparation Technique

Structural and magnetic properties of rare earth substituted Co-Zn ferrites are greatly dependent on fabrication technique. A goal common to all the ferrites is the common formation of the spinel structure. Today, the large majority of ferrite powders are made by the conventional Ceramic process or Solid State Reaction method. Most non-conventional process involves producing the powder by a wet method. Among these methods, some are [Goldman, 1999] Co-precipitation, Organic precursors, Sol-gel synthesis, Spray-drying, Freeze-drying, Glass crystallization etc.

In the present research, we prepared our sample $Co_{0.25}Zn_{0.75}Yb_xFe_{2-x}O_4$ [Where x = 0.00, 0.02, 0.04, 0.06 and 0.08] by Solid state reaction technique.

3.3.1 Solid State Reaction Method

In the solid state reaction method, the required composition is usually prepare from the appropriate amount of raw mineral oxides or carbonates by crushing, grinding and milling [Kittel, 1996]. Solid state reaction occurs between apparently regular crystal lattices, in which the kinetic motion is very much restricted and it depends on the presence of lattice defects [Nelson and Riley, 1945]. In solid state reaction method, appropriate amounts of two or more component of chemical compounds are carefully grinded together and mixed thoroughly in mortar with pestle or ball milling with appropriate homogenization. Solid oxides do not usually react together at room temperature over normal time scale and it is necessary to heat them at much higher temperatures.

The ground powders are then calcined in air or oxygen at a temperature above 700°C. Sometime this process is continued until the mixture is converted into the correct crystalline phase. The calcined powders are then further crushed into fine powders. The pellets or disc shaped and toroid shaped samples are made of these calcined powders using uniaxial or iso-static pressure. Sintering is carried out in the solid state, at temperatures between 700 - 1600°C, for times of typically 1- 5 hours and in various atmospheres (e.g. Air, O_2 and N_2) [Sikder *et. al.*, 2011; Sarout Noor, 2011] . The overall preparation process generally comprised of the following four major steps are Preparing a mixture of desired composition , Pre sintering the mixture to form ferrite, Converting the Raw ferrite into powder then pressing the powder and Sintering.

3.4 Sample Preparation

High purity powders of Co_3O_4 (99.9%), ZnO (99.9%), Yb_2O_3 (99.9%), Fe_2O_3 (99.9%) were used as the raw materials. The exact amounts of compounds were calculated for each composition. Using those raw materials were weighed and mixed thoroughly by hand milling. During hand milling, few drops of acetone were added to increase the degree of mixing. The mixture was pre-sintered at 850ºC for 2 hours. The calcined powder again was crashed into fine powders. From the fine powders, toroid and disk-shaped samples were prepared and sintered at 1150° C for 3 hours. After

sintering the sample we got the final product and we studied the electrical and magnetic properties of the desired sample.

3.4.1 Calculation for Sample Preparation

For the polycrystalline $Co_{0.25}Zn_{0.75}Yb_xFe_{2-x}O_4$ [Where x=0.00, 0.02, 0.04, 0.06 and 0.08] arrangement we used Co_3O_4, ZnO, Yb_2O_3 and Fe_2O_3. The weight percentage of the oxide to be mixed for various samples was calculated by using formula:

$$\text{Weight \% of oxide} = \frac{M.wt \cdot of\ oxide \times required\ weight of the sample}{Sum\ of\ Mol.wt.of\ each\ oxide\ in\ a\ sample}$$

To get exact amount of each of the compounds the detail calculations are shown in following three tables.

Table 3.1: Atomic /molecular mass of raw materials

Name of compound/atom	Molecular / Atomic mass(g/mol)
Co_3O_4	240.80
ZnO	81.39
Yb_2O_3	394.08
Fe_2O_3	159.69
Co	58.933
Zn	65.38
Yb	173.04
Fe	55.845
O	15.999

Table 3.2 Calculation of total mass of the composition.

Composition	**Mass of the sample (g)**
$Co_{0.25}Zn_{0.75}Fe_2O_4$	(58.933×.25)+(65.38×.75)+(55.845×2)+ (15.999×4)=239.454
$Co_{0.25}Zn_{0.75}Yb_{0.02}Fe_{1.98}O_4$	(58.933×.25)+(65.38×.75)+(173.04×.02)+ (55.845×1.98)+(15.999×4)=241.798
$Co_{0.25}Zn_{0.75}Yb_{0.04}Fe_{1.96}O_4$	(58.933×.25)+(65.38×.75)+(173.04×.04)+ (55.845×1.96)+(15.999×4)=244.142
$Co_{0.25}Zn_{0.75}Yb_{0.06}Fe_{1.94}O_4$	(58.933×.25)+(65.38×.75)+(173.04×.06)+ (55.845×1.94)+(15.999×4)=246.485
$Co_{0.25}Zn_{0.75}Yb_{0.08}Fe_{1.92}O_4$	(58.933×.25)+(65.38×.75)+(173.04×.08)+ (55.845×1.92)+(15.999×4)=248.829

Table 3.3: Calculation for 20 g sample preparation

Composition	Need of Co_3O_4(g)	Need of ZnO(g)	Need of Fe_2O_3(g)	Need of Yb_2O_3(g)
$Co_{0.25}Zn_{0.75}Fe_2O_4$	(240.8×0.25×20)/(3×239.454) = 1.676	(81.39×0.75×20)/239.454 = 5.098	(159.69×2×20)/(2×239.454) = 13.337	N/A
$Co_{0.25}Zn_{0.75}Yb_{0.02}Fe_{1.98}O_4$	(240.8×0.25×20)/(3×241.798) = 1.659	(81.39×0.75×20)/241.798 = 5.049	(159.69×1.98×20)/(2×241.798) = 13.076	(394.08×0.02×20)/(2×241.798) = 0.325
$Co_{0.25}Zn_{0.75}Yb_{0.04}Fe_{1.96}O_4$	(240.8×0.25×20)/(3×244.142) = 1.644	(81.39×0.75×20)/244.142 = 5.00	(159.69×1.96×20)/(2×244.142) = 12.820	(394.08×0.04×20)/(2×244.142) = 0.645
$Co_{0.25}Zn_{0.75}Yb_{0.06}Fe_{1.94}O_4$	(240.8×0.25×20)/(3×246.485) = 1.628	(81.39×0.75×20)/246.485 = 4.953	(159.69×1.94×20)/(2×246.485)= 12.568	(394.08×0.06×20)/(2×246.485) = 0.959
$Co_{0.25}Zn_{0.75}Yb_{0.08}Fe_{1.92}O_4$	(240.8×0.25×20)/(3×248.829) = 1.613	(81.39×0.75×20)/248.829 = 4.906	(159.69×1.92×20)/(2×248.829) = 12.322	(394.08×0.08×20)/(2×248.829) = 1.266

3.4.2 Mixed and Milled the Samples (Hand Milling)

Samples were weighed according to the calculation and then mixed thoroughly by solid state reaction method. Each of the compositions was grinded for four hours using agate mortar and pestle. The following figure shows the hand milling set up.

Figure 3.1: Raw materials in agate mortar with pestle

3.4.3 Pre-sintering the Mixture to form Ferrite

Pre-sintering is a process of obtaining a homogeneous and pure sample of mixed powders by heating them for a certain time at a high temperature below the sintering temperature. It is done to increase the strength green compact and remove the lubricants and binders added during blending. During the Pre-sintering stage, the reaction of Fe_2O_3 with metal oxide/carbonate (say, MeO or $MeCO_3$) takes place in the solid state to form spinel according to the reactions:

$$MeO + Fe_2O_3 \longrightarrow MeFe_2O_4 \text{ (Spinel)}$$

$$Fe_2O_3 + MeCO_3 \longrightarrow MeFe_2O_4 + CO_2$$

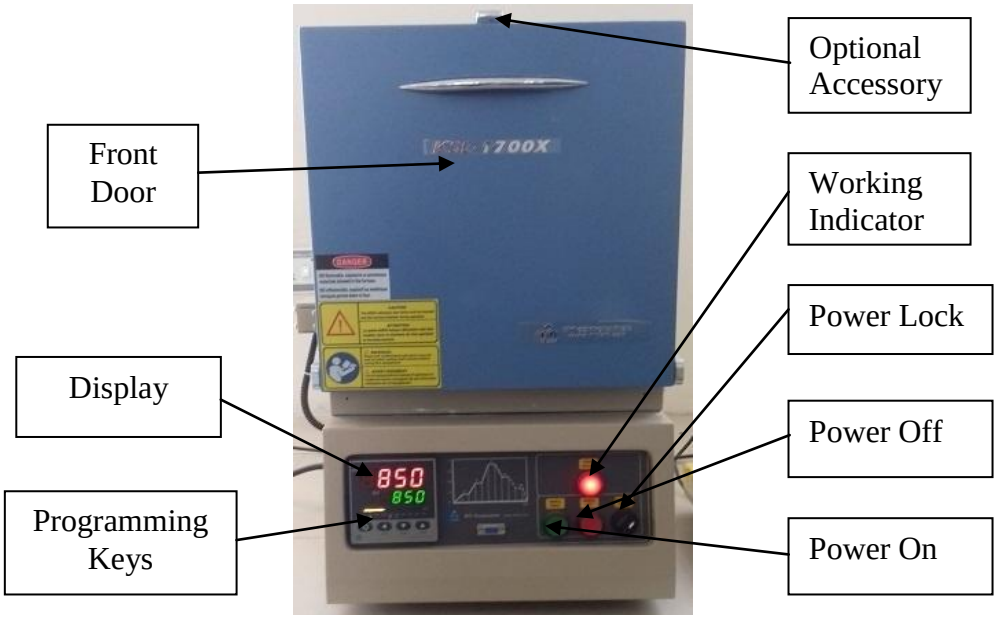

Figure 3.2: Furnace (*KSL-1700X* made in USA) in the solid state physics laboratory, (KUET)

3.4.4 Pressing or Extrusion

Powder pressing is the compaction of powders into a geometric form. Pressing is usually performed at room temperature. This creates a solid part called a green compact. The strength of this pressed, unsintered part, (green strength), is dependent on compactability, binders may be used to increase compactability.

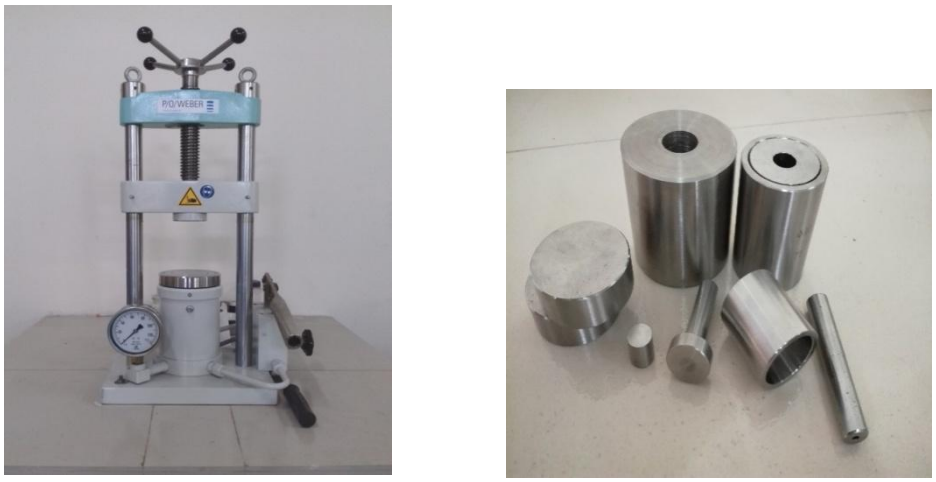

Figure 3.3: Hydraulic press and dies for preparing sample

Table 3.4: Various Shape and size of $Co_{0.25}Zn_{0.75}Yb_xFe_{2-x}O_4$ sample

Shape	Weight (gm)	Name of the sample: $Co_{0.25}Zn_{0.75}Yb_xFe_{2-x}O_4$ [Where x=0.00, 0.02, 0.04, 0.06 and 0.08]					Purpose
		X=0.00	X=0.02	X=0.04	X=0.06	X=0.08	
Ring	1	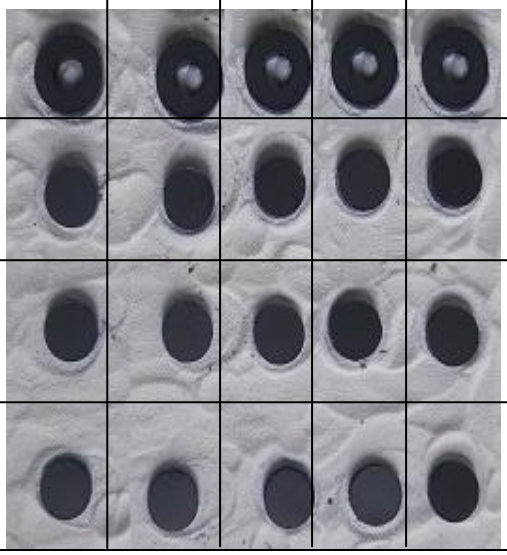					Permeability
Pellet	0.6						VSM, XRD
Pellet	0.4						Dielectric, Resistivity
Pellet	0.3						SEM

3.4.5 Sintering

Sintering is a process of compacting and forming a solid by heat treatment. In this process the atoms in the materials diffuse across the boundaries of the particles, fusing the particles together and creating one solid piece. Sintering process takes places without melting the sample i.e. heating the sample below its melting point. Sintering is the final step in which sintering temperature, sintering time as well as the atmosphere of the furnace play very important role on the magnetic property of final samples.

KSL-1700X-S Furnace

KSL-1700X-S is a compact design high temperature muffle furnace designed for maximum energy saving (<1KW at 10°C/min).It is an ideal tool for materials annealing and sintering in research laboratory.

- The furnace consists of high quality alumina fiber brick and MoSi2 heating elements with double layer case.
- Gas inlet and venting port are installed for using at oxygen or inert gas riched atmosphere.
- Design of sliding down door is for loading sample at easy.

- The furnace temperature is controlled by high precision SCR(Silicon Controlled Rectifier) digital controller with accuracy +/-1°C and 30 segments programmable up to 1700°C.

Figure 3.4: High Temperature Muffle Furnace (KSL-1700X-S) at Solid State Physics Lab, KUET

Illustration of Temperature Segment Setting for Sintering

The $Co_{0.25}Zn_{0.75}Yb_xFe_{2-x}O_4$ sample was sintered at 1150°C. High Temperature Muffle Furnace (KSL-1700X-S) at Solid State Physics Lab, KUET was used for sintering the sample. According to the Furnace operational manual the temperature Control Program was taken with 6-segments as shown in Figure 3.5.

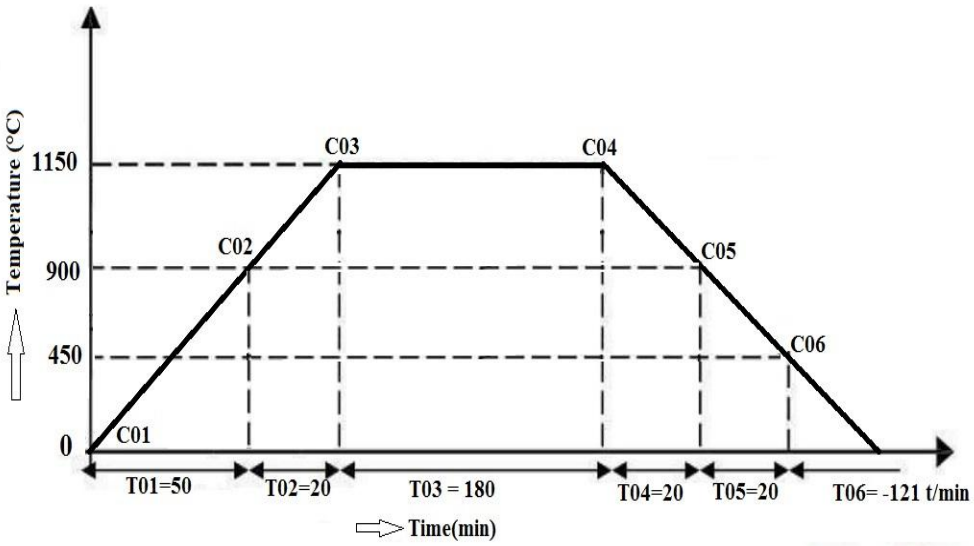

Figure 3.5: Graphical presentation of temperature control program segments

3.5 Sample Preparation at a glance

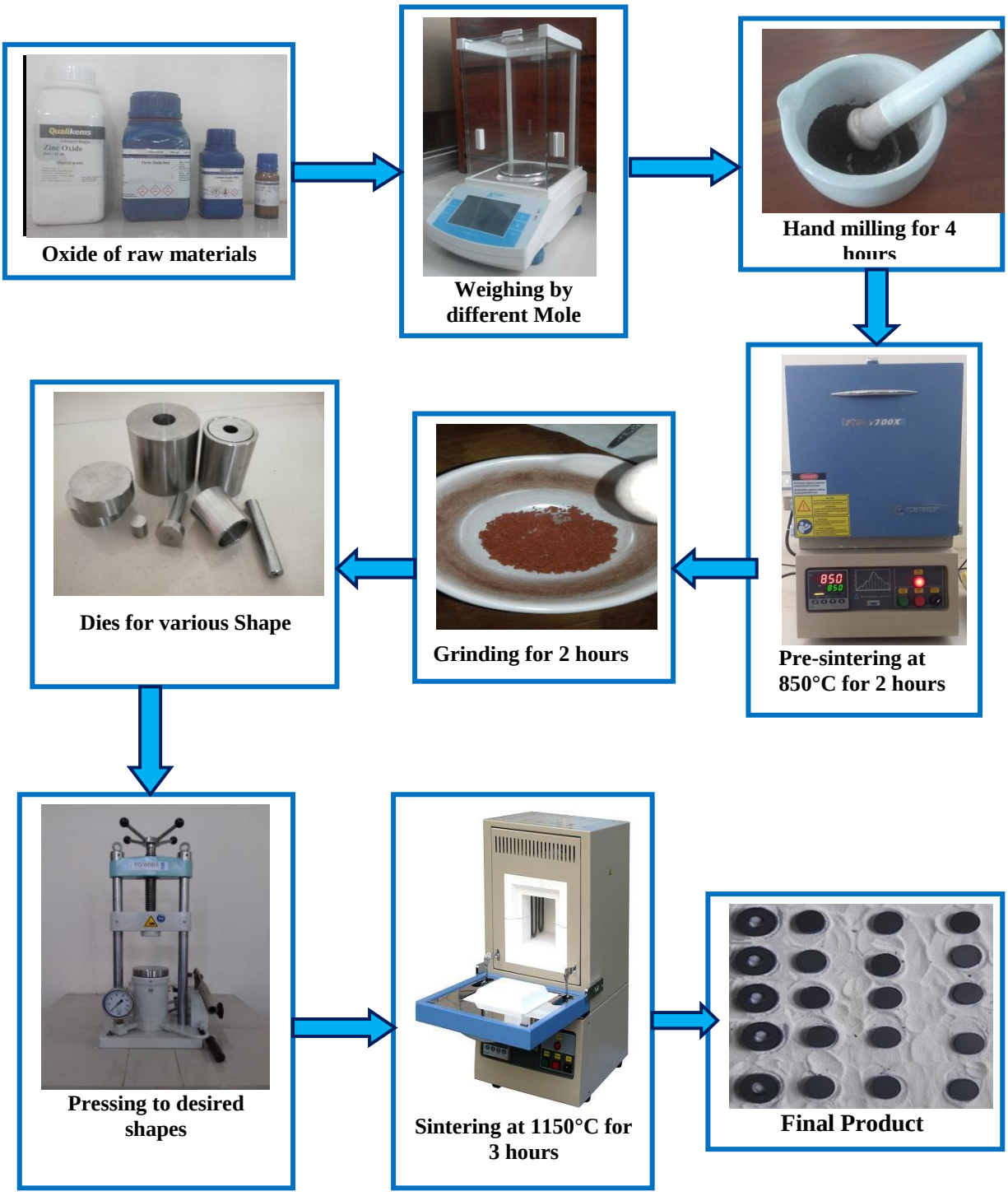

Table 3.5: Temperature Control Program with 6-segments

Prompt	Input Data	Description
C01	0	Initial Temperature
T01	50	Furnace took 50 min from 0-900° C in the 1st segment
C02	900	Target temperature of the 1st heat-up stage
T02	20	Furnace took 20 min from 900-1150° C in the 2nd segment
C03	1150	Target temperature of the 3rd heat-up stage
T03	180	Furnace kept 180 minutes at 1150°C in the 3rdsegment
C04	1150	Target temperature of the fourth stage
T04	20	Cooling time 20 minutes from 1150-900°C
C05	900	Target temperature of the fifth cooling stage
T05	20	Cooling time 20 minutes from 900-450°C
C06	450	Temperature of the sixth stage
T06	-121	Program end, Out-put power off. Furnace cooling down naturally. (T06 = -121 is an order to stop running)

3.6 X-ray Diffraction

X-ray diffraction (XRD) is a rapid analytical technique primarily used for phase identification of a crystalline material and can provide information on unit cell dimensions. It provides precise knowledge of the lattice parameter as well as the substantial information on the crystal structure of the material under study.XRD is based on constructive interference of monochromatic X-ray diffraction from a crystalline sample where crystalline substances act as three-dimensional diffraction gratings with grating constant equal to the spacing of planes in the crystal lattice.

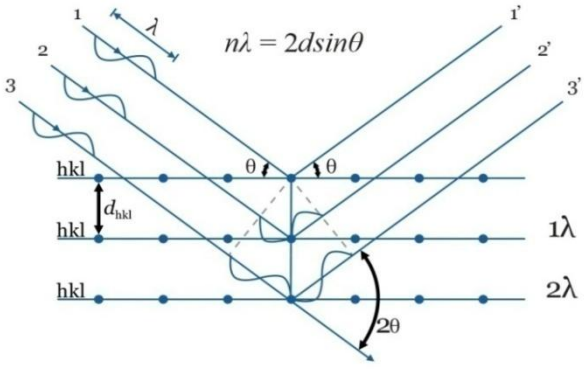

Figure 3.6: Bragg diffraction of x-rays from successive planes of atoms

The interaction of the incident X-rays with the sample produces constructive interference when satisfying the Bragg's condition:

$$2d \sin \theta = n\lambda \qquad (3.1)$$

This law relates the wavelength of electromagnetic radiation to the diffraction angle and the lattice spacing in a crystalline sample. Typically, this is achieved by comparison of d-spacing with standard reference patterns.

3.6.1 Different Parts of the PHILIPS X'Pert PRO XRD System

In this research, Phillips X'pert PRO X-ray diffractometer of Atomic Energy Centre, Dhaka was used. The wavelength of the used X-ray is (λ = 1.5418 Å) and is of the same order of magnitude as that of the lattice constant of crystals and this makes it so useful in structural analysis of crystal structure.

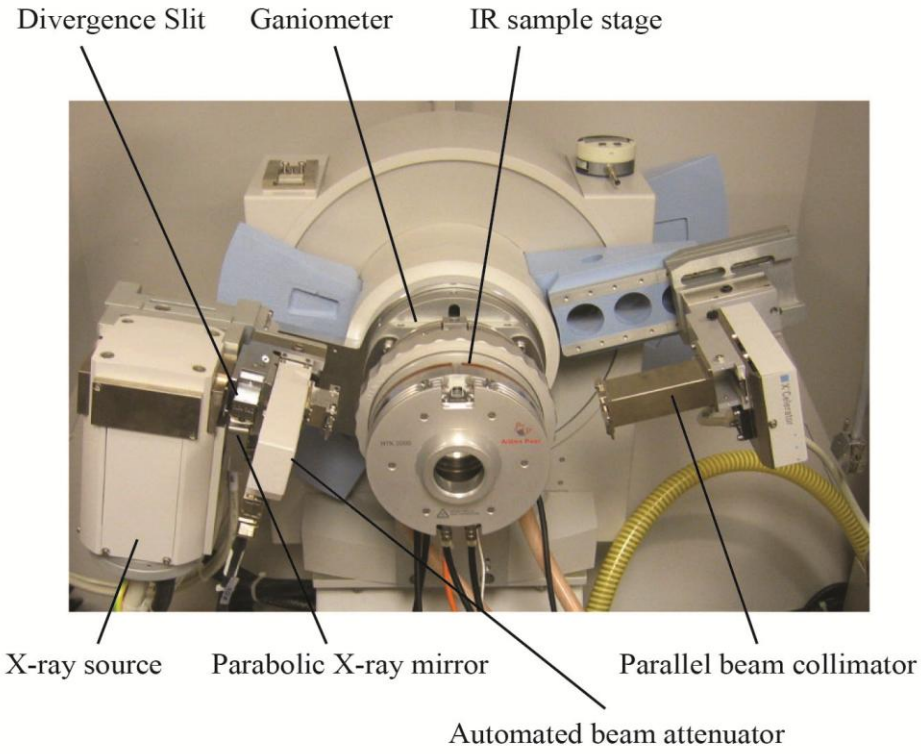

Figure 3.7: Internal arrangement of a PHILIPS X' Pert PRO X-ray diffractometer

3.6.2 Interpretation of the XRD data

The XRD data consisting of θ_{hkl} and d_{hkl} values corresponding to the different crystallographic planes are used to determine the structural information of the samples like lattice parameter and constituent phase. Lattice parameters of Co-Zn ferrites

samples were determined. Normally, lattice parameter of an alloy composition is determined by the Debye-Scherrer method after extrapolation of the curve. We determine the lattice spacing (interplanerdistance), d using these reflections from the equation which is known as Bragg's Law.

$$2d_{hkl}\sin\theta = \lambda$$

$$\text{i.e. } d_{hkl} = \frac{\lambda}{2\sin\theta} \quad , \qquad (3.2)$$

Where λ is the wavelength of the X-ray, θ is the diffraction angle and n is an integer representing the order of the diffraction.

3.6.3 Lattice Parameter

The lattice parameter for each peak of each sample was calculated by using the formula:

$$a = d_{hkl} \times \sqrt{h^2 + k^2 + l^2} \qquad (3.3)$$

Where h, k, l are the indices of the crystal planes. We get d_{hkl} values from the computer using software "X' Pert HJGHS CORE". So we got ten 'a' values for ten reflection planes such as a_1, a_2, a_3 ….. etc. Determine the exact lattice parameter for each sample, through the Nelson-Riley extrapolation method. The values of the lattice parameter obtained from each reflected plane are plotted against Nelson-Riley function [Tahir Abbas *et al.*, 1995].The Nelson-Riley function F (θ) can be written as

$$F(\theta) = \frac{1}{2}\left[\frac{\cos^2\theta}{\sin\theta} + \frac{\cos^2\theta}{\theta}\right], \qquad (3.4)$$

Where, θ is the Bragg's angle. Now drawing the graph of 'a' vs. F(θ) and using linear fitting of those points will give us the exact lattice parameter 'a'. This value of 'a' at F(θ) = 0 or θ = 90° .These 'a's are calculated with an error estimated to be ± 0.0001Å.

3.6.4 X-ray Density and Bulk Density

X-ray density, ρ_x was also calculated usual from the lattice constant. The relation between ρ_x and 'a' is as follows,

$$\rho_x = \frac{ZM}{Na^3} \qquad (3.5)$$

where M is the molecular weight of the corresponding composition, N is the Avogadro's number ($6.023X10^{23}$ $mole^{-1}$), 'a' is the lattice parameter and Z is the number of molecules per unit cell, (Z = 8 for the spinel cubic structure).

The bulk density was calculated considering a cylindrical pellet of mass (m) and volume (V) of the pellets using the relation

$$\rho_B = \frac{mass\ of\ the\ sample}{volume\ of\ the\ sample} = \frac{m}{V} = \frac{m}{\pi r^2 \mathrm{h}} \quad (3.6)$$

Where m is the mass of the pellet sample, r is the radius and h is the thickness of the pellet.

3.6.5 Porosity

Porosity is the amount of spaces in between sediments. Porosity is a parameter which is inevitable during the process of sintering of oxide materials. It is noteworthy that the physical and electromagnetic properties are strongly dependent on the porosity of the studied samples. Therefore an accurate idea of percentage of pores in a prepared sample is prerequisite for better understanding of the various properties of the studied samples to correlate the microstructure property relationship of the samples under study.

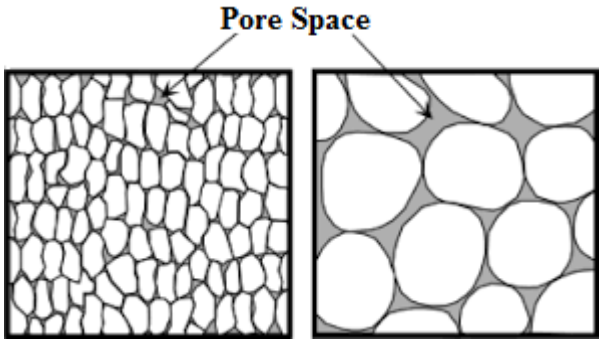

Figure 3.8: Porosity

The porosity of a material depends on the shape, size of grains and on the degree of their storing and packing. The difference between the bulk density ρ_B and X-ray density ρ_x gave us the measure of porosity. Percentage of porosity has been calculated using the following relation [Smit and Wijin, 1959]

$$P\% = \left(1 - \frac{\rho_B}{\rho_x}\right) \times 100\% \quad (3.7)$$

3.7 Surface Morphology and Microstructure

The microstructural study was performed in order to have an insight of the grain structures. The samples of different compositions were chosen for this purpose. The samples were visualized under a High-resolution Scanning Electron Microscope (SEM) images. Average grain sizes of the samples were determined from SEM

micrographs by linear intercept technique [Hossain, 1998]. To do this, several random horizontal and vertical lines were drawn on the micrographs. Therefore, we counted the number of grains intersected and measured the length of the grains along the line traversed. Finally the average grain size was calculated.

3.7.1 Scanning Electron Microscope (SEM)

Scanning Electron Microscope (SEM) is a type of electron microscope that creates various images by scanning the surface of the sample. SEM is one kind of surface morphology where a high energy beam of electrons are focused on the surface of a sample and detecting signals from the interaction of the incident electron with the sample's surface. In Scanning Electron Microscope process signals come from the primary beam impinging upon the sample and from other interactions within the sample near the surface. The SEM is capable of producing high resolution images of a sample surface in its primary use mode, secondary electron imaging. Characteristic x-rays are emitted when the primary beam causes the ejection of inner shell electrons from the sample and are used to tell the elemental composition of the sample. The back-scattered electrons emitted from the sample may be used alone to form an image.

Figure 3.9: Scanning Electron Microscope (SEM)

3.8 Permeability Measurement

3.8.1 Wayne Kerr Precision Impedance Analyzer

The Wayne Kerr Technologies 6500B series of Precision Impedance analyzer provides impedance measurement capability of components from 20Hz up to 120

MHz. A comprehensive range of functions enables a component to be accurately characterized over a wide frequency range with a choice of Analysis and meter modes allowing swept, single and repetitive measurements. The Graphical User Interface (GUI) combined with the large touch screen TFT display enables measurement parameters to be modified easily and quickly Figure 3.10. The instrument may be remotely controlled using the GPIB or LAN interface.

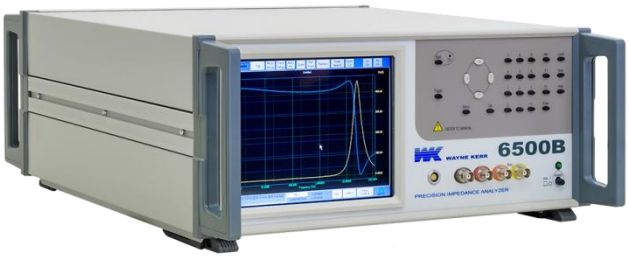

Figure 3.10: Wayne Kerr Impedance analyzer (6500B series) in solid state physics laboratory, KUET.

Table 3.6

AC Measurement parameters
➢ Impedance (Z) ➢ Inductance (L) ➢ Resistance (R) ➢ Capacitance (C) ➢ Phase Angle (θ) ➢ Dissipation Factor (D) ➢ Quality Factor (Q) ➢ Reactance (X) ➢ Conductance (G) ➢ Susceptance (B) ➢ Admittance (Y)

Figure 3.11: Complex permeability measurement by Wayne Kerr Precision Impedance analyzer

A comprehensive range of AC functions enables a wide range of components to be measured accurately. Each measurement displays two user selectable components,

which allow specific component characteristics to be monitored. Any of the following parameters can be measured and displayed.

3.8.2 Permeability

To determine the frequency dependent complex permeability of the studied samples, toroid shape samples were used. The polished samples were cleaned with acetone and then coiled with copper wire. The measurements of complex permeability of the toroid shaped samples were performed at room temperature in the frequency range from 1 KHz to 100MHz. The real part, μ'and imaginary part, μ" of the complex permeability were measured using the following formulas

$$\mu' = \frac{L_S}{L_0} \tag{3.8}$$

$$\text{and} \quad \mu'' = \mu' \cdot \tan\delta_M \tag{3.9}$$

Here, L_S is the inductance of the sample and $L_0 = \frac{\mu_0 N^2 S}{\pi \bar{d}}$ derived theoretically for the samples. $L_0$is the inductance of the winding coil except the sample, N represents the number of turns of the coil (N = 5), S indicates the cross sectional area of the toroid samples as given below,

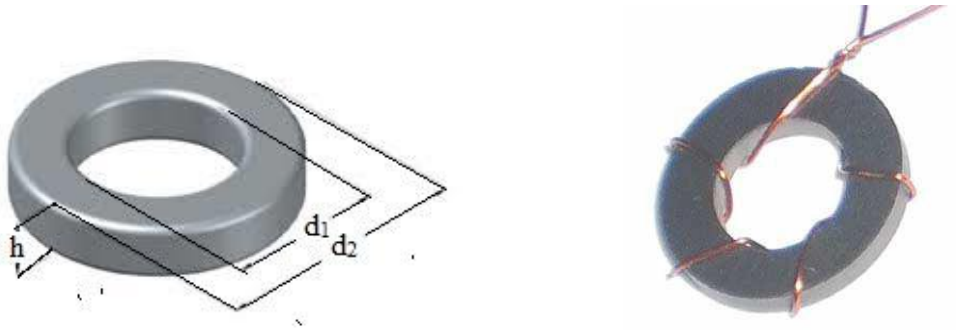

Figure 12: Toroid sample with winding coil.

$$S = d \times h \tag{3.10}$$

$$and, \quad d = \frac{d_2 - d_1}{2} \tag{3.11}$$

Where, d_1 is the inner radius, d_2 is the outer radius and h is the height of the ring. Again, $\bar{d}$ indicates the mean diameter of the toroidal sample and can be written as,

$$\bar{d} = \frac{d_1 + d_2}{2} \tag{3.12}$$

Again, Quality Factor

$$Q = \frac{1}{\tan\delta_M} \tag{3.13}$$

And relative quality factor

$$RQF = \frac{\mu'}{\tan\delta_M} \tag{3.14}$$

3.9 Dielectric Properties

Ceramics are mostly covalently bonded material hence electrically non conductive or insulator. Importance of particular property depends on the application demand. For instance, dielectric strength is an important parameter for application of ceramic as insulators used in power transmission line, load bearing general insulators, in house hold appliances etc. In this kind of applications where frequency do not exceed 1kHz, the break down strength, measured in kV/cm, together with mechanical strength are important factors. The dielectric constant ($\varepsilon^{/}$) or loss factor ($\varepsilon^{//}$) does not matter much. On the other hand, for capacitors and electronics application just the opposite required. The values of $\varepsilon^{/}$ and $\varepsilon^{//}$ are of prime importance, not only their room temperature values but also as function of frequency. These are intrinsic properties of material; especially of polycrystalline ceramic can be modified by doping, micro structural variation.

3.9.1 Dielectric Constant

Dielectric constant measurements were done by using Wayne Kerr Impedance Analyzer 6500B. The overall dielectric constant ($\varepsilon^{/}$) of an insulator material as given by the relation:

$$D = \varepsilon_0 E = \varepsilon_0 \varepsilon' E \tag{3.15}$$

D represents the electric displacement, E the electric field in the dielectric, $\varepsilon^{/}$ the dielectric constant and ε_0 permittivity of the vacuum. The dielectric constant $\varepsilon^{/}$ is an intrinsic property of a material and a measure of the ability of the material to store electric charge relative to vacuum. It is measured directly from the capacitance of a capacitor in which the material is used as electrode separator or dielectric. The capacitive cell, the dielectric constant ($\varepsilon^{/}$), total charge (q) and capacitance C can be developed as follows:

$$\varepsilon' = \frac{D}{\varepsilon_0 E} = \frac{\frac{Q}{A}}{\frac{\varepsilon_0 V}{d}} \tag{3.16}$$

$$\therefore Q = \frac{\varepsilon_0 \varepsilon' AV}{d} = CV \tag{3.17}$$

Where $C = \frac{\varepsilon_0 \varepsilon' A}{d}$ (3.18)

Here A represents the area of the capacitive cell, d its thickness, C is the capacitance of the material, V the voltage across the cell and ε_0 the material permittivity in vacuum. Thus $\varepsilon^{/}$ represents the ratio of the permittivity or charge storage capacity relative to air or vacuum as dielectric.

$$\varepsilon' = \frac{cd}{\varepsilon_o A}, \tag{3.19}$$

where c is the capacitance of the pellet in Farad, d the thickens of the pellet in meter , A the cross-sectional area of the flat surface of the pellet in m^2 and ε_o the constant of permittivity for free space. Dielectric measurement as a function of frequency in the range 100Hz-120MHz at room temperature were carried out by using Wayne Kerr Impedance Analyzer 6500B in conjunction with a laboratory made furnace which maintain the desired temperature with the help of a temperature controller.

3.9.2 Dielectric Loss

Dielectric loss often attributed to ion migration, ion vibration & deformation and electric polarization. Ion migration is particularly important and strongly affected by temperature and frequency. The losses due to ion migration increase at low frequency and the temperature increases. By definition,

$$tan\delta = \frac{\varepsilon''}{\varepsilon'} \tag{3.20}$$

The imaginary part of dielectric constant (ε″) of the sample was calculated using relation: ε″ = ε′ tanδ; where tanδ is the dielectric loss tangent.

3.10 Vibrating Sample Magnetometer (VSM)

A vibrating Sample Magnetometer (VSM) is a scientific instrument to measure the magnetization of a sample under an external magnetic field. It operates on the Faraday's low of induction.

The working principle of VSM is the measurement of the electromotive force induced by a magnetic sample when it is vibrated at a constant frequency in the presence of a static and uniform magnetic field. In a VSM, a sample is placed within a uniform magnetic field H which induces a magnetization M in the sample. It is then

vibrated sinusoidally, which creates a corresponding vibration of the magnetic flux in the pick-up coils nearby and induces a sinusoidal voltage.

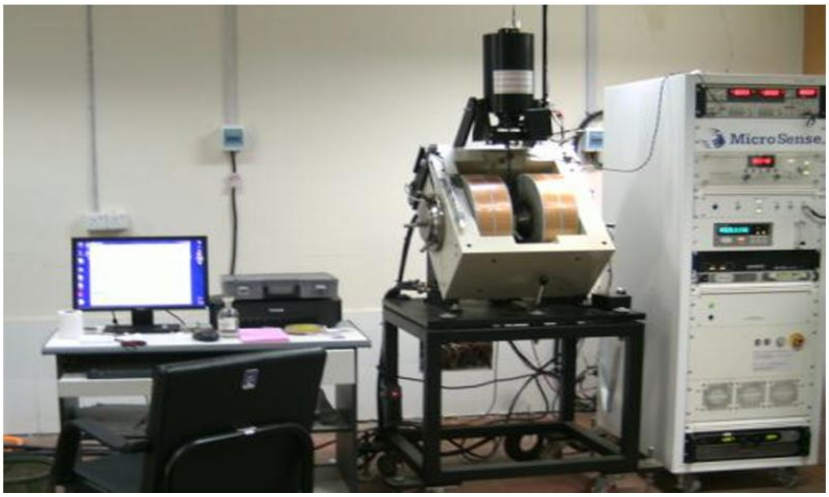

Figure 3.13: Microsense Vibrating Sample Magnetometer

The amplitude of the ac voltage is proportional to the samples magnetic moment and measured by a lock-in amplifier [Forner, 1959]. In this study, Microsense VSM model EV7 at Atomic Energy Commission, Dhaka was used to determine the magnetic properties of the samples. A small part of the samples were 9 to 11 mg used and was made to avoid movements inside the sample holder. To understand the ferromagnetic effect, full-cycle hysteresis loops were obtained over a wide range of field from -10 KOe to +10 KOe.

3.11 DC Resistivity

Sintered pellet specimens were used to determine resistivity. Electrical conductivity of the samples was studied after silver pasting the two polished surfaces of each pellet as shown in Figure 3.14. The temperature dependent ρ_{DC} from room temperature up to 500K were carried out by using two probe method and was estimated by using the following relation

$$\rho_{DC} = \frac{R\pi r^2}{l} \qquad (3.21)$$

Where R is the resistance, r is the radius and l is the thickness of the samples.

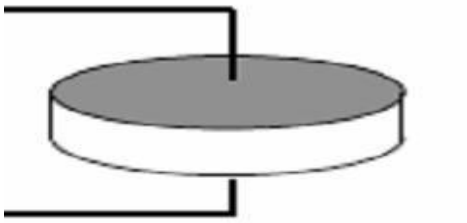

Figure 3.14: Schematic arrangement on the silver pasted pellet sample

CHAPTER IV

RESULTS AND DISCUSSION

RESULTS AND DISCUSSION

4.0 Introduction

Rare earth oxides are good additives to change the magnetic and electrical properties of ferrites. The magnetic and electrical properties can be changed by substitutions various kinds of divalent cations or relatively small amount of rare earth ions [Ahmed *et al.,* 2005]. In this chapter, magnetic, electrical and structural properties of Ytterbium (Yb) doped Co-Zn ferrites are investigated. The Yb substituted polycrystalline $Co_{0.25}Zn_{0.75}Yb_xFe_{2-x}O_4$, [Where x = 0.00, 0.02, 0.04, 0.06 and 0.08] have been prepared by standard solid state reaction technique. XRD patterns of Co-Zn confirm single phase and formation of cubic structure. The magnetic properties such ac complex permeability of the ferrites investigated in the frequency range (1 KHz to 120 MHz) by Wayne Kerr Impedance Analyzer. Surface morphology was measured by SEM (model JEOL JSM 7600F) and hysteresis loop was analyzed by VSM. Dielectric properties, DC resistivity and other electrical properties of the samples are studied.

4.1 X-Ray Diffraction Analysis of $Co_{0.25}Zn_{0.75}Yb_xFe_{2-x}O_4$ Ferrites

XRD analysis is a useful way to get the structural information of a material. To study the structural view of Yb doped Co-Zn ferrites we used Philips X'pert PRO X-ray diffractometer. For XRD analysis we used powder sample of $Co_{0.25}Zn_{0.75}Yb_xFe_{2-x}O_4$ ferrites sintered at 1150°C for 3 hours. In this case, X-ray diffractometer equipped with Cu-K_α radiation (λ = 1.5418 Å) in the range of 2θ = 20° to 65° in steps of 0.02°.

4.1.1 Phase Analysis

The structural view or the various phases of Yb doped Co-Zn ferrites were confirmed from XRD analysis. Figure 4.1 shows the X-ray diffraction patterns of Yb doped Co-Zn ferrites. Figure 4.1 shows eight sharp peaks and the peaks can be indexed as (111), (220), (311), (222), (400), (422), (511), and (440). No impurity peak is found and all the peaks in pattern match well with the theoretically generated. Here, all the miller indices of a peak are either all odd or even, which confirmed that the samples are spinel lattice with cubic structure. This also confirms the homogeneity of the studied samples. All the reflection peaks were identified and indexed in good

agreement with the referred database of the International Centre for Diffraction Data (ICDD).

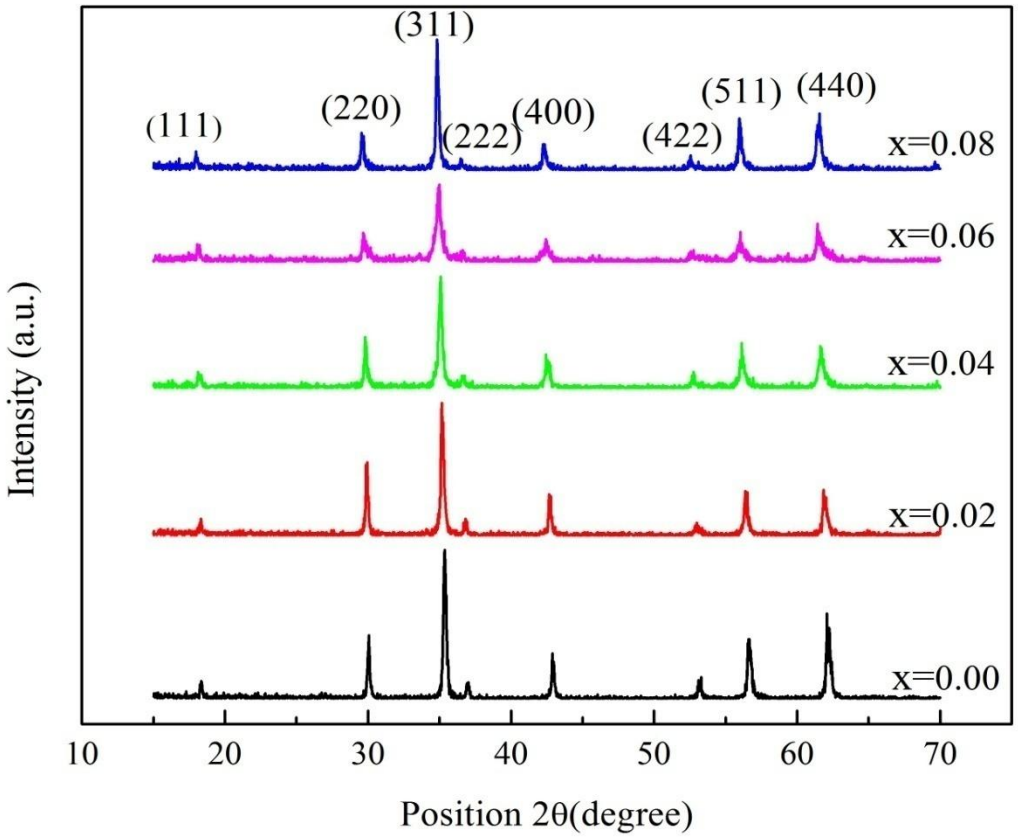

Figure 4.1: X-ray diffraction spectra of $Co_{0.25}Zn_{0.75}Yb_xFe_{2-x}O_4$, [Where x=0.00, 0.02, 0.04, 0.06 and 0.08] ferrites sintered at 1150°C for 3 hours.

From the X-ray data we calculated the position of any peaks and using Bragg's law ($2d \sin\theta = n\lambda$) we got the values of interplanar spacing (d). The position of the X-ray peaks and their corresponding miller indices for the studied samples investigated are given in Table 4.1.

Table 4.1: Position of the X-ray peaks and corresponding miller indices for $Co_{0.25}Zn_{0.75}Yb_xFe_{2-x}O_4$ [Where x=0.00, 0.02, 0.04, 0.06 and 0.08] ferrites.

Content	Miller indices of the X-ray peaks and their position 2θ in degree							
	(111)	(220)	(311)	(222)	(400)	(422)	(511)	(440)
X=0.00	18.35	30.02	35.36	36.9	42.9	53.21	56.63	62.05
X=0.02	18.29	29.91	35.13	36.83	42.67	52.95	56.40	61.83
X=0.04	18.16	29.78	35.06	36.68	42.47	52.74	56.12	61.62
X=0.06	18.10	29.64	34.98	36.60	42.39	52.70	56.00	61.43
X=0.08	17.97	29.52	34.81	36.50	42.3	52.55	55.99	61.58

4.1.2 Lattice Parameters

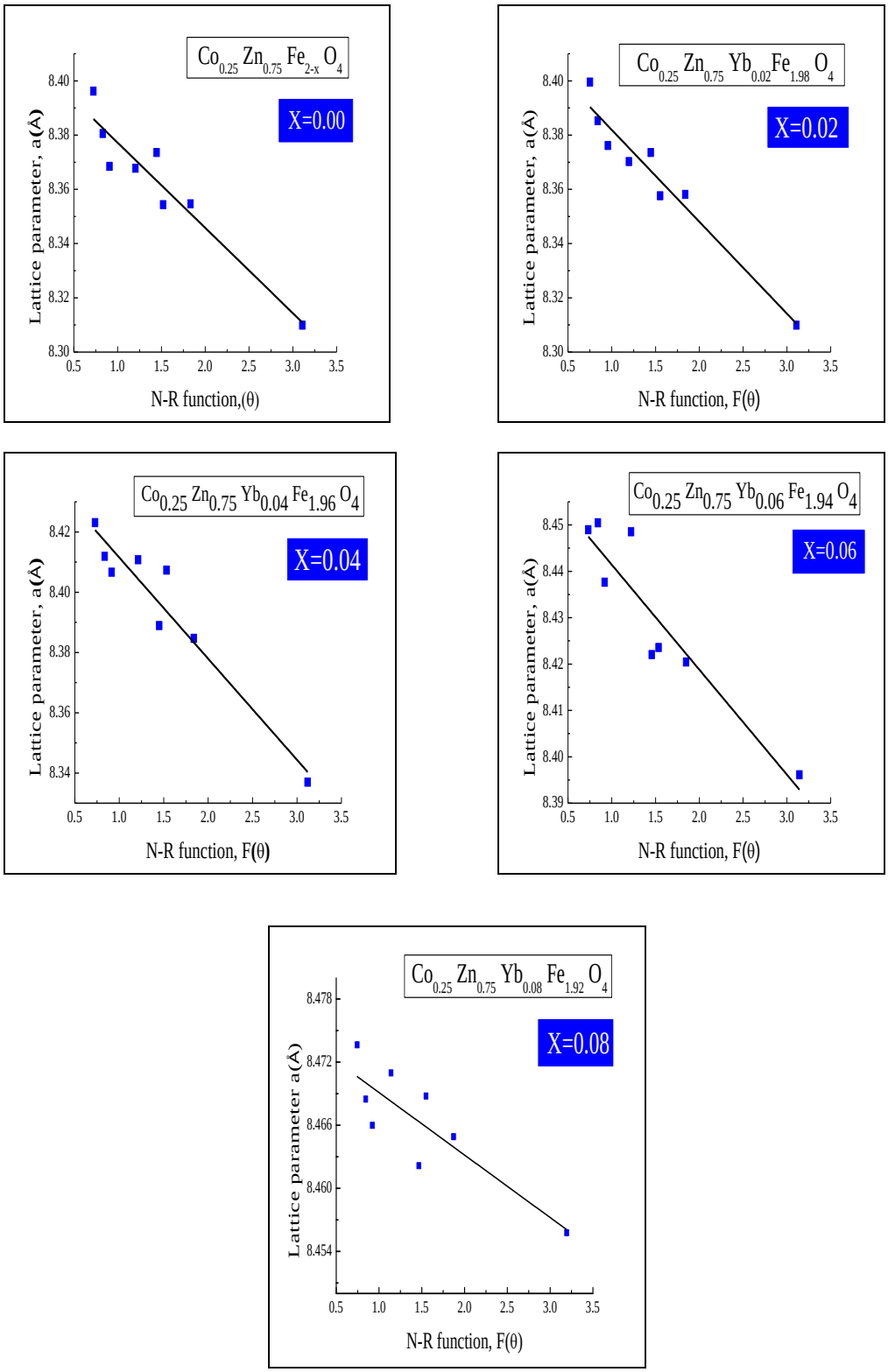

Figure 4.2: Variation of lattice parameter 'a' with N-R function and determination of exact lattice parameter of $Co_{0.25}Zn_{0.75}Yb_xFe_{2-x}O_4$ ferrites.

The values of the lattice parameter obtained from each plane with the help of Nelson-Riley extrapolation method [equation 3.4]. For each of the reflection plane we got individual F(θ) and individual lattice parameter. Figure 4.2 shows the representative curves for Yb content of extrapolating N-R function. The least square linear fitting gives the precise lattice parameter as an intercept on the Y-axis. From each graph between lattice parameter and N-R function we got five Average values of lattice parameter for five ferrite samples. Now we can compare the effect of Yb substitution on the lattice parameter of $Co_{0.25}Zn_{0.75}Yb_xFe_{2-x}O_4$ ferrites as shown in Figure 4.3.

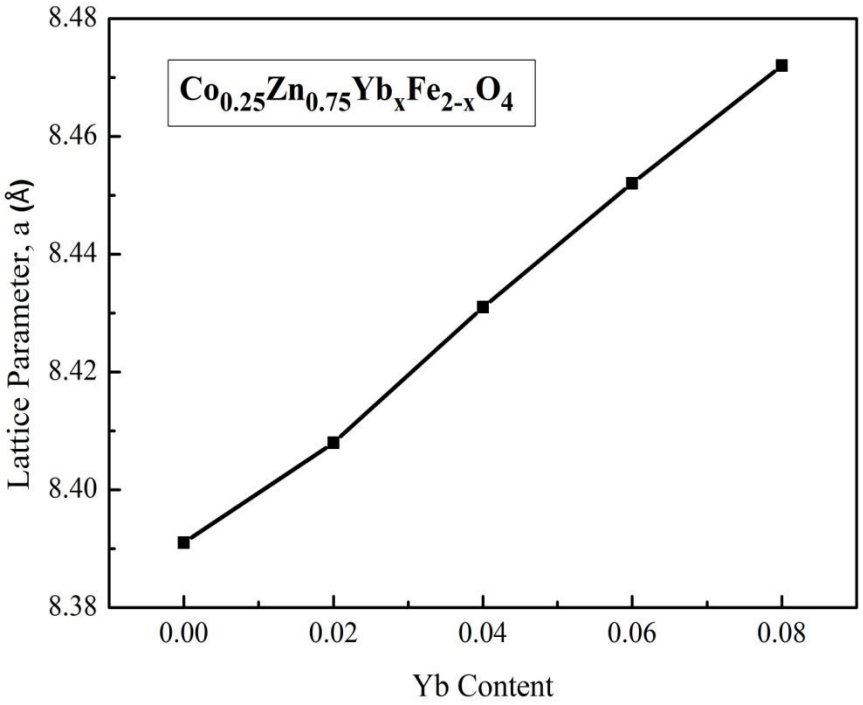

Figure 4.3: Variation of lattice parameters with the increase of Yb content.

From Figure 4.3 it is clear that the lattice parameter (a) increases with increasing Yb^{3+} content. The values of lattice parameters for various $Co_{0.25}Zn_{0.75}Yb_xFe_{2-x}O_4$ ferrites are listed in Table 4.2. This increase in lattice constant can be explained in the basis of ionic radii. The ionic radii of the cations used in $Co_{0.25}Zn_{0.75}Yb_xFe_{2-x}O_4$ are Co^{2+}(0.72 Å), Zn^{2+}(0.82 Å), Yb^{3+} (1.03Å) and Fe^{3+} (0.64Å). Here the ionic radius of Yb is greater than the ionic radii of Fe. For this reason doping of big atom increases the lattice parameter. This enhancement of lattice parameter is attributed to Yb^{3+} with larger ionic radius which replaces Fe^{3+} having smaller radius. It is well known that the distribution of cations on the octahedral B-sites and tetrahedral A-sites determines to a great extent the physical, electrical and

magnetic properties of Co-Zn ferrites These changes in lattice parameters with Yb^{3+} content indicate that the present system obeys the Vegard's law [Vegard's, 1921]. Thus the introduction of larger ions in the ferrite results in an increase of the distance between the magnetic ions. There exists a correlation between the ionic radius and the lattice constant, the increase of the lattice parameter is proportional to the increase of the ionic radius.

4.1.3 Density and Porosity

Density of ferrite samples plays an important role in the determination of magnetic and electric properties. It is well known that high permeability could be achieved by increasing the density of the ferrites. The X-ray density calculated from the determined lattice parameter and bulk density measured from the ratio of mass and volume of all the $Co_{0.25}Zn_{0.75}Yb_xFe_{2-x}O_4$ ferrite samples. The calculated values of the X-ray density (ρ_x), bulk density (ρ_B) and porosity (P %) of the present ferrites are listed in Table 4.2. The X-ray density or theoretical density ρ_x was found to be increased from 5.38 to 5.44 g/cm^3 with the increase in Yb^{3+} substitution. Here the X-ray density is related to the molecular weight (M) and lattice constant (a).The increase in X-ray density might be due to the greater atomic mass of Yb^{3+} (173.04 amu) than that of Fe^{3+} (55.85 amu).

Table 4.2: Data of the lattice parameter (a), X-ray density (ρ_x), bulk density (ρ_B), porosity (P%) of $Co_{0.25}Zn_{0.75}Yb_xFe_{2-x}O_4$, [Where x=0.00, 0.02, 0.04, 0.06 and 0.08] ferrites sintered at 1150°C for 3 hours.

Content	a (Å)	ρ_x (gm/cm^3)	ρ_B (gm/cm^3)	Porosity (%)
X= 0.00	8.391	5.38	4.99	7.13
X= 0.02	8.408	5.40	4.96	8.13
X= 0.04	8.431	5.41	4.92	8.90
X= 0.06	8.452	5.42	4.88	9.94
X= 0.08	8.472	5.44	4.82	11.30

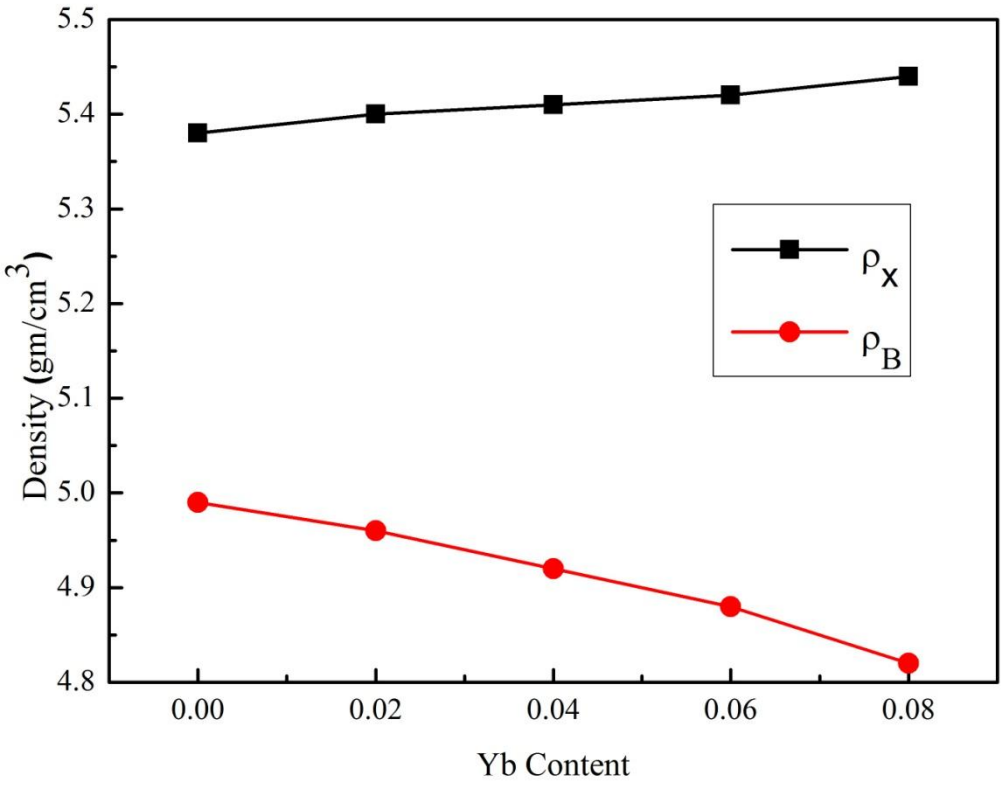

Figure 4.4: Variation of bulk density and X-ray density as a function of Yb content

It is observed that bulk density is lower than the X-ray density shown in Figure 4.4. This may be due to the existence of pores which were formed and developed during the sample preparation or sintering process. The bulk density slightly decreases with increasing rare earth ion Yb^{3+} and the X-ray density increases continuously with increasing x-content.

It is observed that porosity increases monotonically with increasing Yb^{3+} content. It was difficult to remove these closed porosities completely due to the evaporation of constituents specially Zn. It is known that the porosity of the samples come from two sources, intragranular porosity and intergranular porosity. The intergranular porosity mainly depends on the grain size [Yang *et al.*, 2006]. The porosity which is intrinsic for any oxide material plays an important role in the deciding the magnetic and electrical properties due to pore spaces.

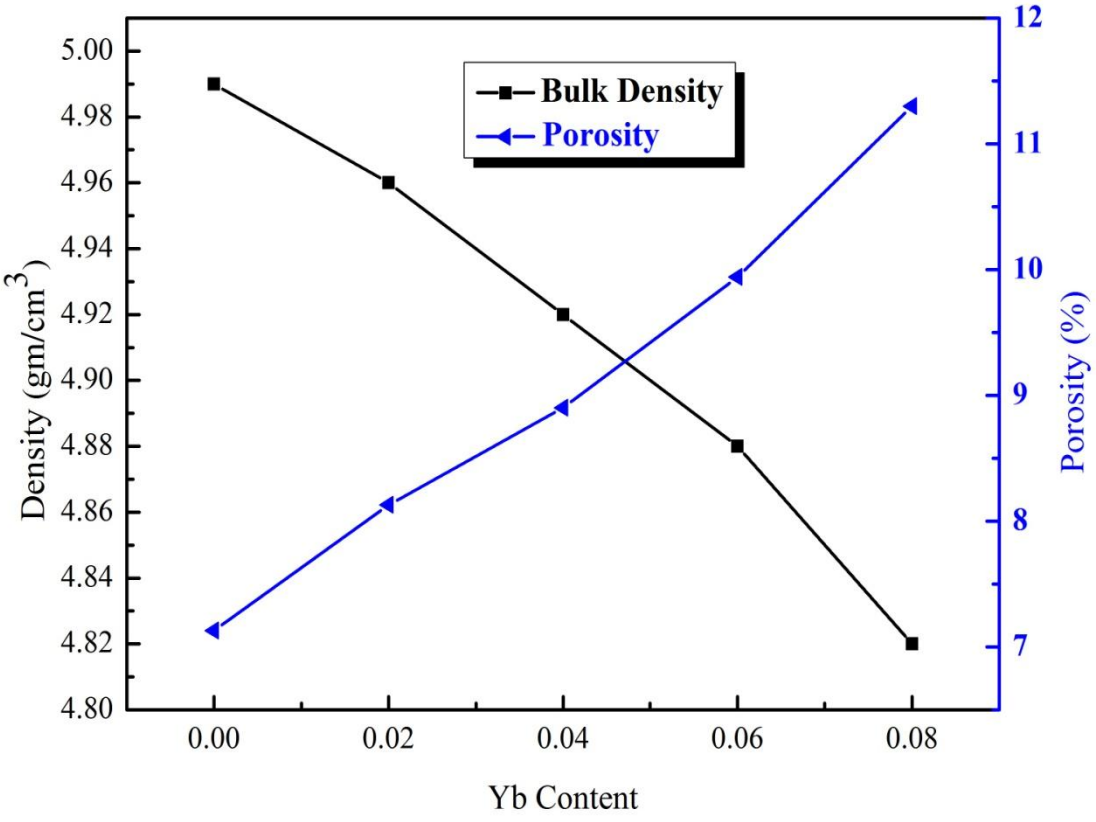

Figure 4.5: Variation of bulk density and porosity as a function of Yb content for various $Co_{0.25}Zn_{0.75}Yb_xFe_{2-x}O_4$ Ferrites sintered at 1150°C/3hrs.

The enhancement of bulk density is due to activated diffusion process triggered by the excess vacancies created by Fe^{3+} deficiency. It may be also be mentioned that reduction Fe^{2+} due to Fe^{3+} deficiency is expected to increase the resistivity of the samples. This density plays an important role on the magnetic propertqies especially on the structure sensitive property such as permeability and flux density. Table 4.2 shows the results of lattice parameter, theoretical density, and bulk density calculated porosity. It is observed from the Table 4.2 that porosity decreases monotonically with increasing Fe-deficiency in constant with bulk density which shows reverse behavior in Figure 4.5.

4.2 Microstructures of $Co_{0.25}Zn_{0.75}Yb_xFe_{2-x}O_4$ Ferrites

Structural, magnetic and electrical properties of ferrites are sensitively depending on the microstructure of the ferrite samples.

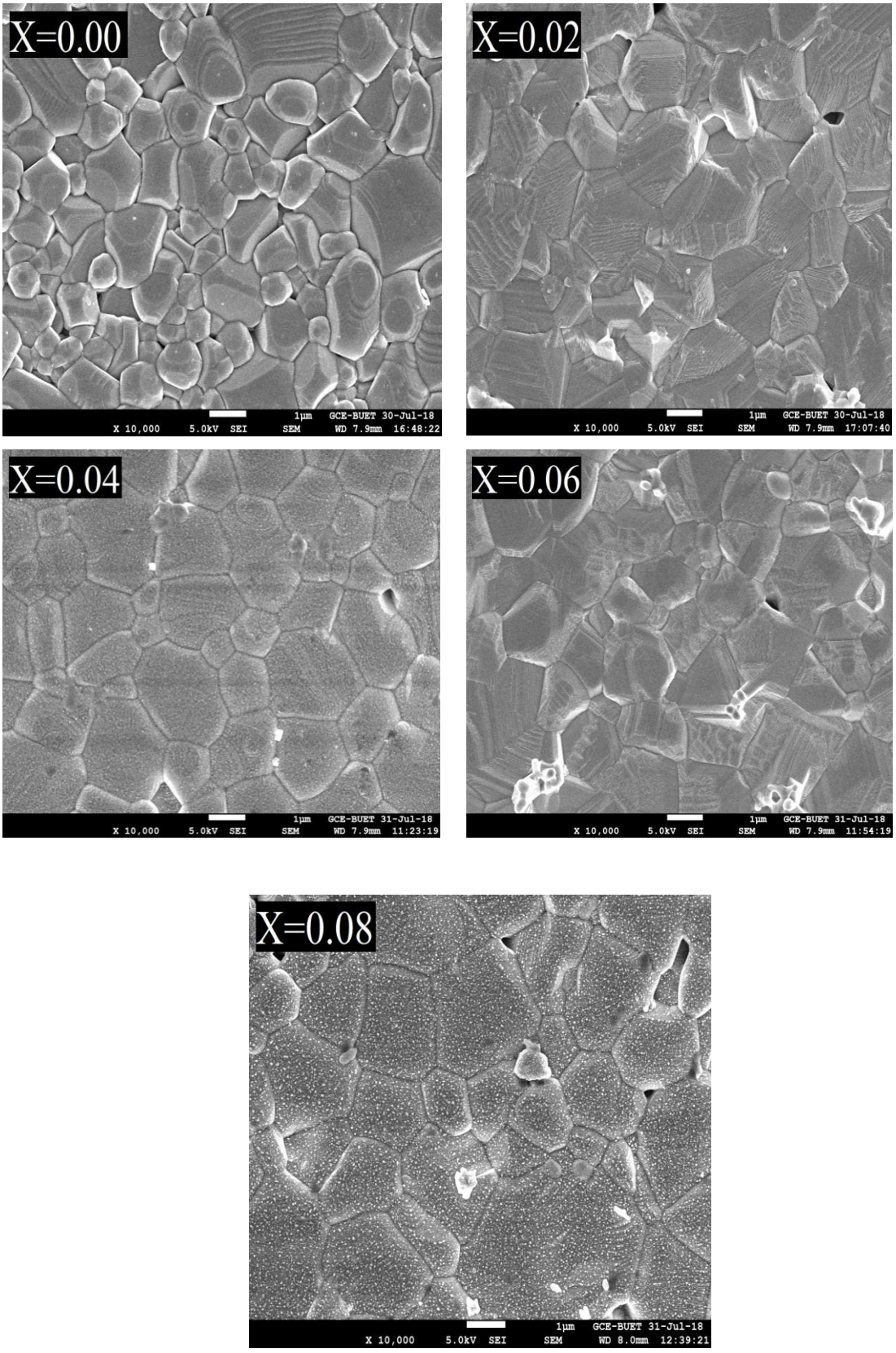

Figure 4.6: SEM micrographs of $Co_{0.25}Zn_{0.75}Yb_xFe_{2-x}O_4$, [Where x=0.00, 0.02, 0.04, 0.06 and 0.08] ferrites sintered at 1150°C/3hrs.

Figure 4.6 shows the microstructure of sintered pellets. From these above figures the average grain size increases gradually with increasing Yb content. It occurred due to the fact that sintering of ferrites might be assisted by a liquid phase that drew the particles together due to capillary forces and enabled more densification. The average grain size was calculated using Image J software from the SEM micrograph and has been shown in Table 4.3.

Table 4.3: Average grain size for $Co_{0.25}Zn_{0.75}Yb_xFe_{2-x}O_4$ ferrites.

Name of the sample	Contents	Average grain size(μm)
$Co_{0.25}Zn_{0.75}Fe_2O_4$	X = 0.00	1.29
$Co_{0.25}Zn_{0.75}Yb_{0.02}Fe_{1.98}O_4$	X = 0.02	1.73
$Co_{0.25}Zn_{0.75}Yb_{0.04}Fe_{1.96}O_4$	X = 0.04	1.98
$Co_{0.25}Zn_{0.75}Yb_{0.06}Fe_{1.94}O_4$	X = 0.06	2.15
$Co_{0.25}Zn_{0.75}Yb_{0.08}Fe_{1.92}O_4$	X = 0.08	2.35

Here the average grain size was estimated in the range from 1.29 μm to 2.35 μm. The crystal grain growth depends on grain boundaries migrating and larger crystal grains swallowing the small ones. Grain growth is closely related to the grain boundary mobility. Recrystallization and grain growth involve the movement of grain boundaries. It facilities the grain growth by increasing the rate of cations inter diffusion as a result of its segregation to the grain boundaries [Mendelson, 1969, Saroaut Noor *et. al.* 2010]. The grain growth, being a result of interparticle mass transport, appears to be dominated by the bimodal diffusion mechanism [Gupta and Coble, 1968]. The behavior of grain growth reflects the competition between the driving force for grain boundary movement and the retarding force that drives the grain boundaries to grow over pores. Un-substituted Yb (x = 0) showed the presence of a monophasic homogeneous microstructure with an average grain size 1.29 μm whereas, Yb doped specimens [Figure x = 0.02 to x = 0.08] showed a bi-phasic microstructure constituted of dark ferrite matrix grain and small whitish grain at the grain junction/boundary and also average grain size increase with increasing Yb content. However, the surface morphology was found to be changed from granular to lamellar.

4.3 Magnetic Properties

4.3.1 Variation of Saturation Magnetization at Room Temperature

Figure 4.7 shows the magnetization as a function of applied field for various $Co_{0.25}Zn_{0.75}Yb_xFe_{2-x}O_4$ [Where x = 0.00, 0.02, 0.04, 0.06 and 0.08] samples at room temperature. The hysteresis loops do not show any noticeable hysteresis effect. All samples exhibited low coercivity values indicated that all the samples are family of soft ferrites. The magnetization (M) of all ferrites increases linearly with increasing the applied magnetic field up to 1kOe. After 1kOe the applied field magnetization increases slowly and then saturation occurs. It mentions that all the ferrite samples are in ferromagnetic state and get hysteresis loop for $Co_{0.25}Zn_{0.75}Yb_xFe_{2-x}O_4$ system. It2 is observed that the magnetization increases sharply at very low field (H < 2kOe) which corresponds to magnetic domain reorientation that thereafter increases slowly up to saturation due to spin rotation.

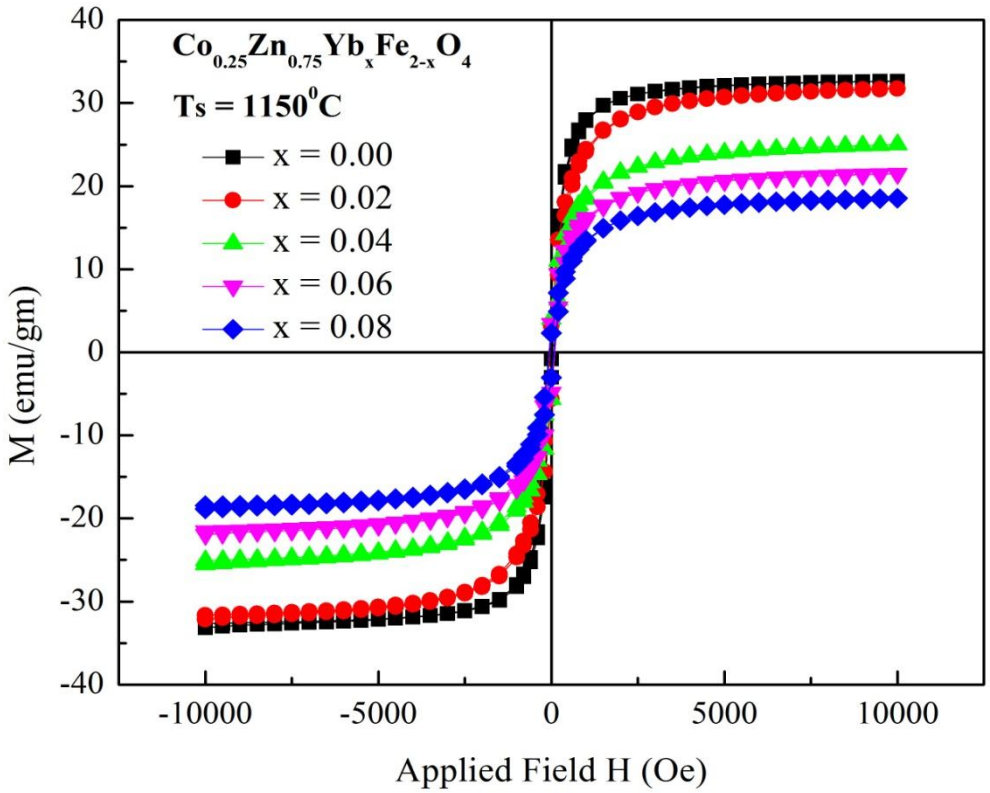

Figure 4.7: Hysteresis loops of $Co_{0.25}Zn_{0.75}Yb_xFe_{2-x}O_4$, [Where x=0.00, 0.02, 0.04, 0.06 and 0.08] ferrites at room temperature.

This magnetization curve nature is connected with soft magnetic behavior of Yb doped Co-Zn ferrites. The slow process of magnetization toward the saturation value is connected with the magnetic anisotropy effect. From the hysteresis loop the saturation magnetization (M_s), coercivity (H_c), remanent magnetization (M_r), magnetic moment in Bohr magneton (μ_B) and the approximate anisotropy constant (K_u) were calculated and listed in Table 4.4.

The value of M_s were found to be decreases with the increasing of Yb^{3+} doped content for all the samples. The decrease in M_s can be explained by the cation distribution in which Yb^{3+} ions can convert some of Fe^{2+} to Fe^{3+} in B-sites. The magnetic moment of Fe^{2+} is less than that of the Fe^{3+}, therefore magnetic moment (μ_B) as well as M_s as shown in Table 4.4. Here the value of effective magnetic moment and radii of Yb^{3+} ions are responsible for decreasing M_s. We know that Fe^{3+}-Fe^{3+} interaction is very strong, when we doped Yb^{3+} ion with replacing Fe^{3+} ion then the interaction between Fe^{3+}-Fe^{3+} decreased. For this reason the M_s decreases with the increasing of the Yb^{3+} doped content.

Table 4.4: Saturation magnetization (M_s), coercivity(H_c), remanent magnetization (M_r), magnetic moment in Bhor magneton (μ_B), and anisotropy constant (K_u) of $Co_{0.25}Zn_{0.75}Yb_xFe_{2-x}O_4$ [where x=0.00, 0.02, 0.04, 0.06, and 0.08] ferrites.

Content	M_s (emu/gm)	H_c (Oe)	M_r (emu/gm)	μ_B	K_u
X = 0.00	32.64	11.90	1.10	1.40	194
X = 0.02	31.74	60.48	4.42	1.37	960
X = 0.04	25.00	81.56	4.84	1.10	1020
X = 0.06	21.48	81.56	4.15	0.95	876
X = 0.08	18.54	67.84	2.68	0.83	629

However, the value of coercivity (H_c) were found to be gradually increased with increasing Yb^{3+} content except x = 0.08 .With the increase in Yb^{3+} content, the residing amount of Yb^{3+} ions at grain boundaries increased. For this reason, the movement of domain walls was more difficult, and hence the coercivity was increased, which distinguish reversible and irreversible types of relaxation due to

Yb^{3+} ions. Irreversible type of relaxation is those are compared an atomic pair which corresponds to irreversible domain wall movements under external field.

The values of anisotropy constant (K_u) were found to be very less than that reported in rare earth doped $CoFe_2O_4$ and showed that grains were not single domains and anisotropy contribution was not uniaxial, but it might be cubic magneto-crystalline anisotropy and hence strong grain to grain interaction were existed in these materials. The values of Bohr magnetron (μ_B) were found to be increased with increasing Yb^{3+}content. This is attributed to the spontaneous magnetization existing in the composites. The spontaneous magnetization of the composites is originated from the unbalanced anti-parallel spins which lead to the net spins [Zhang *et al.,* 2008]. Moreover it has been predicted that in the in the Co-Zn ferrite phases, each ferrite grain is in contact with the ferroelectric grain and this connection is increased with addition of ferrite content and hence M_s and μ_B.

4.3.2 Frequency Dependence of Complex Permeability

Permeability measures the capacity of the substance to take magnetization. It is one of the most important parameter in evaluating the magnetic properties of a material. The magnetic permeability under an oscillatory electromagnetic field is a complex quantity and can be expressed as,

$$\mu = \mu' - i\mu'' \qquad (4.2)$$

where μ' and μ'' are the real and imaginary part of the complex permeability respectively. Complex permeability has been determined as a function of frequency. It was measured over a wide range of frequency from 1 KHz to 120 MHz at room temperature. For all the samples of $Co_{0.25}Zn_{0.75}Yb_xFe_{2-x}O_4$ ferrites we used conventional technique based on the determination of the complex impedance of circuit loaded with toroid shaped sample. With the help of Wayne Kerr Impedance Analyzer we collected 800 data point for initial permeability at different frequency range from 1 KHz to 120 MHz. Among these data some of the values of initial permeability at different frequency range are listed in Table 4.5. For avoiding the noise peak we only took these values of initial permeability at different frequency range from 1MHz to 120MHz. It is seen that μ' remains almost constant until very high frequency (around 50MHz) and then drops rapidly. The fairly constant μ' values over a wide range of frequency region are known as the zone of utility because it demonstrates the compositional stability and quality of the prepared samples.

Table 4.5: Values of initial permeability at different frequency range for $Co_{0.25}Zn_{0.75}Yb_xFe_{2-x}O_4$, [Where x=0.00, 0.02, 0.04, 0.06 and 0.08] ferrites.

Yb Content	μ' at 100Hz	μ'at 10KHz	μ' at 100KHz	μ' at 1MHz	μ' at 10MHz	μ' at 100MHz
X = 0.00	14.07	14.75	14.73	14.55	14.10	12.56
X = 0.02	13.78	14.24	14.24	14.10	13.67	12.17
X = 0.04	12.95	13.88	13.91	13.77	13.31	11.98
X = 0.06	12.60	13.53	13.56	13.47	13.05	11.88
X = 0.08	12.02	12.88	12.94	12.84	12.48	11.12

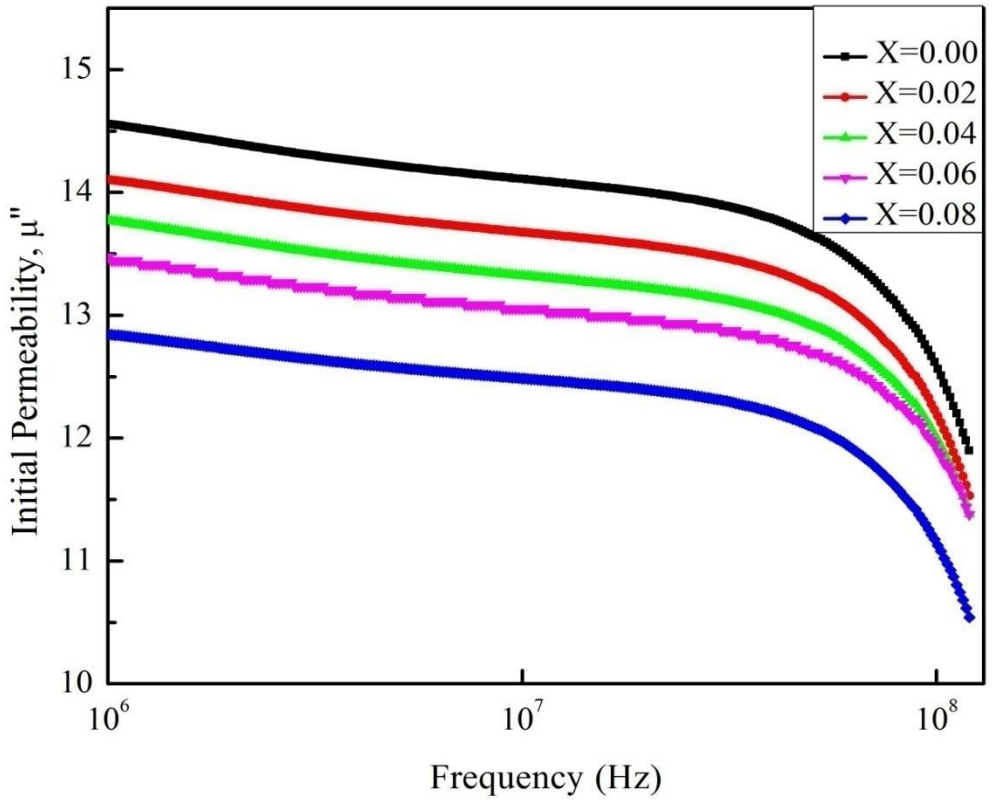

Figure 4.8: Frequency dependent initial permeability of $Co_{0.25}Zn_{0.75}Yb_xFe_{2-x}O_4$, [Where x=0.00, 0.02, 0.04, 0.06 and 0.08] ferrites sintered at 1150°C for 3 hours.

Here the initial permeability remains stable for a long frequency range due to hopping of electron between Fe^{2+} and Fe^{3+}. It could be observed that the initial

permeability decreases significantly with substitution of Yb content. The slightly decrease in initial permeability at x = 0.02 – 0.08 is probably due to minor precipitation of secondary phase $FeYbO_3$. Figure 4.8 shows the variation of μ' with frequency of the system $Co_{0.25}Zn_{0.75}Yb_xFe_{2-x}O_4$ ferrites sintering at 1150°C for constant annealing time 3 hours. The initial permeability of $Co_{0.25}Zn_{0.75}Yb_xFe_{2-x}O_4$ ferrite materials are also depend on many factors like reversible domain wall displacement, domain wall bulging as well as microstructural features, average grain size, intra granular porosity, etc[Smit and Wijn, 1959]. When frequency is low then we get high permeability and when frequency is high then we get permeability is low. Thus, an effective limit of product of frequency and permeability can be established.

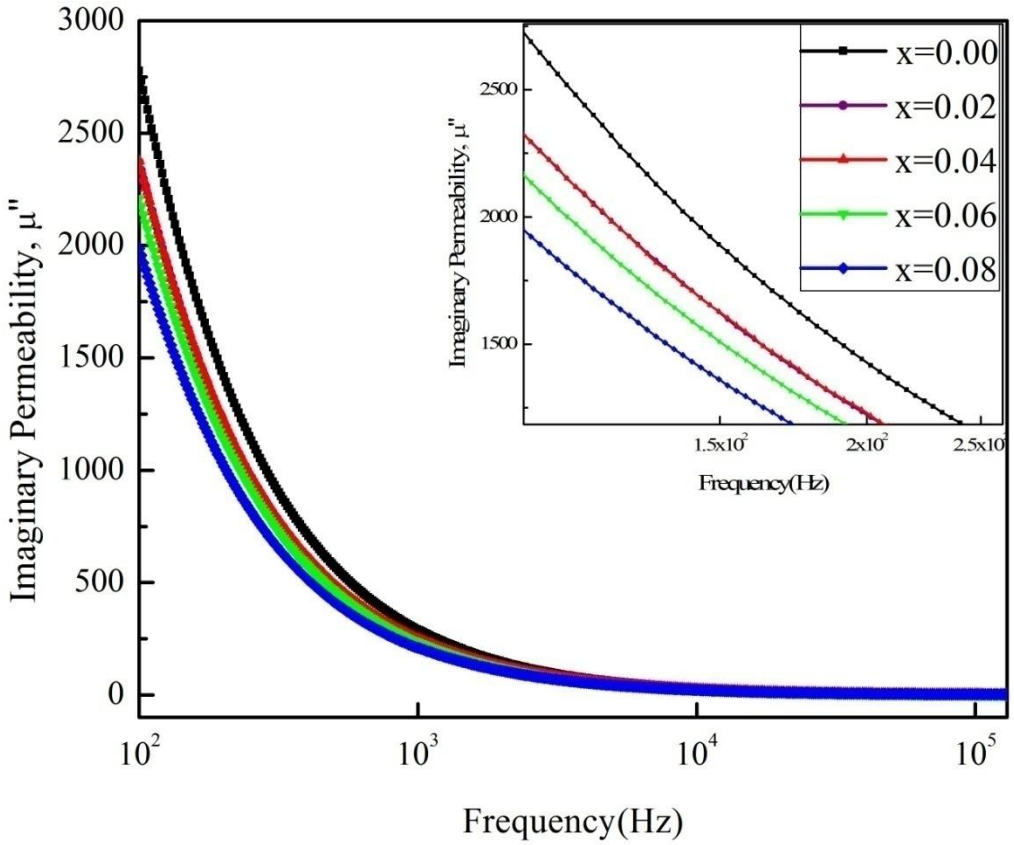

Figure 4.9: Frequency dependent imaginary permeability of $Co_{0.25}Zn_{0.75}Yb_xFe_{2-x}O_4$, [Where x=0.00, 0.02, 0.04, 0.06 and 0.08] ferrites sintered at 1150°C/3 hours.

The imaginary permeability (μ'') were found to be decreased with the frequency and reached a minimum at a certain frequency, where the real permeability (μ') starts to decrease as shown in Figure 4.8 and Figure 4.9. The imaginary permeability initially high at low frequency zone all the samples and then decreases

with increasing frequency almost μ'' constant high frequency range. The grain growth increases with increasing Yb content diminishes the grain boundary, thereby the domain walls can not move easily leads to lower permeability. The decrease in imaginary permeability implies onset of ferromagnetic resonance [Globus *et al.*, 1977]. Also during grain growth pores become fewer, which act as independents to domain wall motion due to pinning wall. At high frequencies at constant μ'' parameters become more significant, the inductors show high impedance and become resistive and dissipate interfacing signals rather than reflecting this source.

4.3.3 Frequency Dependence of Loss Tangent

Loss factor is an important parameter in a soft ferromagnetic material, since the amount of energy wasted on process other than magnetization can prevent the AC applications of a given material. The ratio of μ″and μ′ is equal tanδ representing the losses in the material are a measure of the inefficiency of the magnetic system. The variation of loss factor, tanδ (= μ″/ μ′) with frequency for all samples has been studied. Figure 4.10 shows the variation of loss factor (tanδ) with frequency for various $Co_{0.25}Zn_{0.75}Yb_xFe_{2-x}O_4$, samples sintered at 1150°C holding time 3 hours. The magnetic losses, which cause the phase shift, can be split up into three components: hysteresis losses, eddy current losses and residual losses. This gives the formula $\tan\delta m = \tan\delta_h + \tan\delta_e + \tan\delta_r$. As μ′ is the initial permeability which is measured in presence of low applied magnetic field, therefore, hysteresis losses vanish at very low field strengths.

Thus at low field the remaining magnetic losses are due to eddy current losses and residual losses. Residual losses are independent of frequency. Eddy current losses increase with frequency and are negligible at very low frequency. Eddy current loss can be expressed energy loss per unit volume and □ is the resistivity [Valenzuela, 1994]. To keep the eddy current losses constant as frequency is increased; the resistivity of the material chosen must increase as the square of frequency. Eddy currents are not problem in the Co-Zn ferrites until higher frequencies are encountered because they have very high resistivity about $10^5\Omega$-cm to $10^8\Omega$-cm [Brailsford, 1996]. The ferrite microstructure is assumed to consist of grains of low resistivity separated by grain boundaries of high resistivity. Thicker grain boundaries are preferred to increase the resistance

It is clear from the Figure 4.10 that the value of tanδ is less frequency dependent in the frequency range from 1kHz to 100MHz. Therefore, it is concluded that the synthesized composites have excellent performance in a wide frequency range and can be used for MLCF application, such as embedded inductors or embedded capacitors.

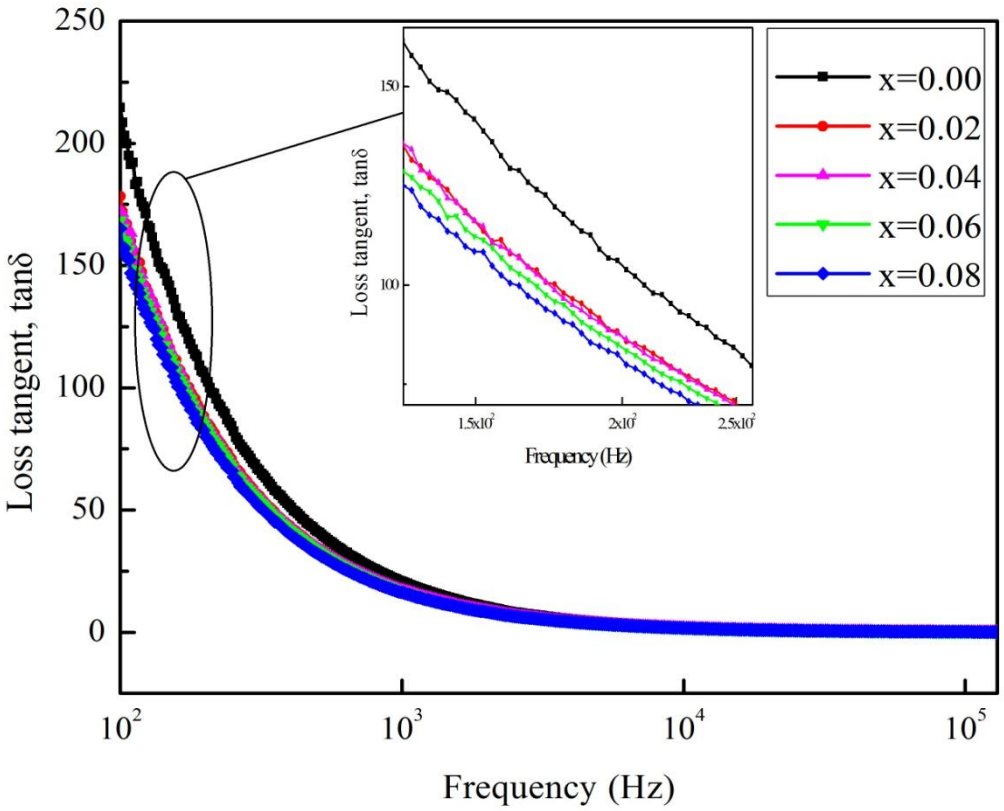

Figure 4.10: Frequency dependent loss factor of $Co_{0.25}Zn_{0.75}Yb_xFe_{2-x}O_4$, [Where x=0.00, 0.02, 0.04, 0.06 and 0.08] ferrites sintered at 1150°C for 3 hours

At lower frequencies, a decrease in magnetic loss is observed. The lag of domain wall motion with respect to the applied magnetic field is responsible for magnetic loss and this is accredited to lattice imperfections [Cullity, 1972].

4.4 Frequency Dependent Dielectric Properties

Figure 4.11 shows the variation of dielectric constant, ε' with frequency for different composition of $Co_{0.25}Zn_{0.75}Yb_xFe_{2-x}O_4$ [Where x=0.00, 0.02, 0.04, 0.06 and 0.08] ferrites sintered at 1150°C/3hrs. Here the dielectric constant was measured over a wide range of frequency from 1 KHz to 120 MHz at room temperature. It can be seen from the Figure 4.11 that the dielectric constant is found to decrease continuously with increasing frequency for all the specimens. The Decrease in

dielectric constant with increasing frequency is a normal behavior of ferrites, which was observed before Mg-Zn ferrite [Jadhav *et al.*, 1999] and Co-Zn ferrite [Kodama, 1999]. The dielectric dispersion is rapid at lower frequency region and it remains almost independent at high frequency side. The effect of rare earth Yb^{3+} substitution into these ferrites has no pronounced effect on the dielectric constant in high frequency, but significantly decreases the dielectric constant in the low frequency range. The dielectric behavior of ferrites may be explained on the basis of the mechanism of the dielectric polarization process and is similar to that of the conduction process. The electronic $Fe^{2+} \leftrightarrow Fe^{3+}$gives the local displacement of electrons in the direction of applied electric field, which induces the polarization in ferrites [ZhenxingYue *et al.*, 2001].

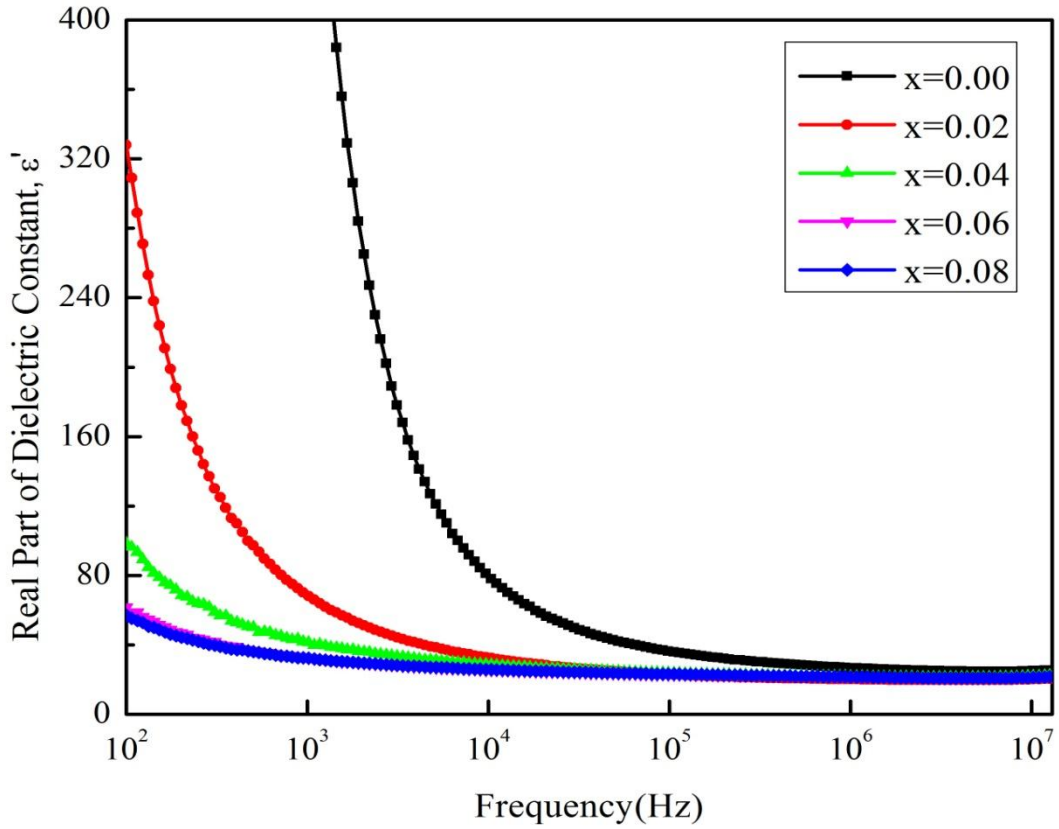

Figure 4.11: Frequency dependent real part of dielectric constant of $Co_{0.25}Zn_{0.75}Yb_xFe_{2-x}O_4$, [Where x=0.00, 0.02, 0.04, 0.06 and 0.08] ferrites sintered at 1150°C for 3 hours.

The magnitude of exchange depends on the concentration Fe^{2+}/Fe^{3+} in pairs present on B-site for the present ferrite. All the samples have high value of $\varepsilon^{/}$ in the order of 10^5 at low frequencies. This could be explained using Koop's

phenomenological theory [Maxwell, 1873; Wanger, 1913] which was based on the Maxwell-Wagner model for the inhomogeneous double layer dielectric structure.
The first layer is the fairly well conducting large ferrite grain which is separated by the second thin layer of the poorly conducting grain boundaries. The grain boundaries of the lower conductivity were found to be ferrite at lower frequencies while ferrite grains of high conductivity are effective at high frequency.

The imaginary part of dielectric constant, ε" was also decreased with increasing frequency as shown in Figure 4.12. At very high frequency the value of ε" becomes so small that it remains independent of applied frequency. The rapid decrease of ε" at lower frequencies can also be explained on the basis of space charge polarization. We know that ferrites are made up of well conducting layer of grains followed by poorly conducting layer of grain boundaries. During the exchange process between Fe^{3+}- Fe^{2+} the electrons have to pass through the grains and grain boundary of the dielectric medium. After that the electrons accumulate at grain boundary and produce space charge polarization.

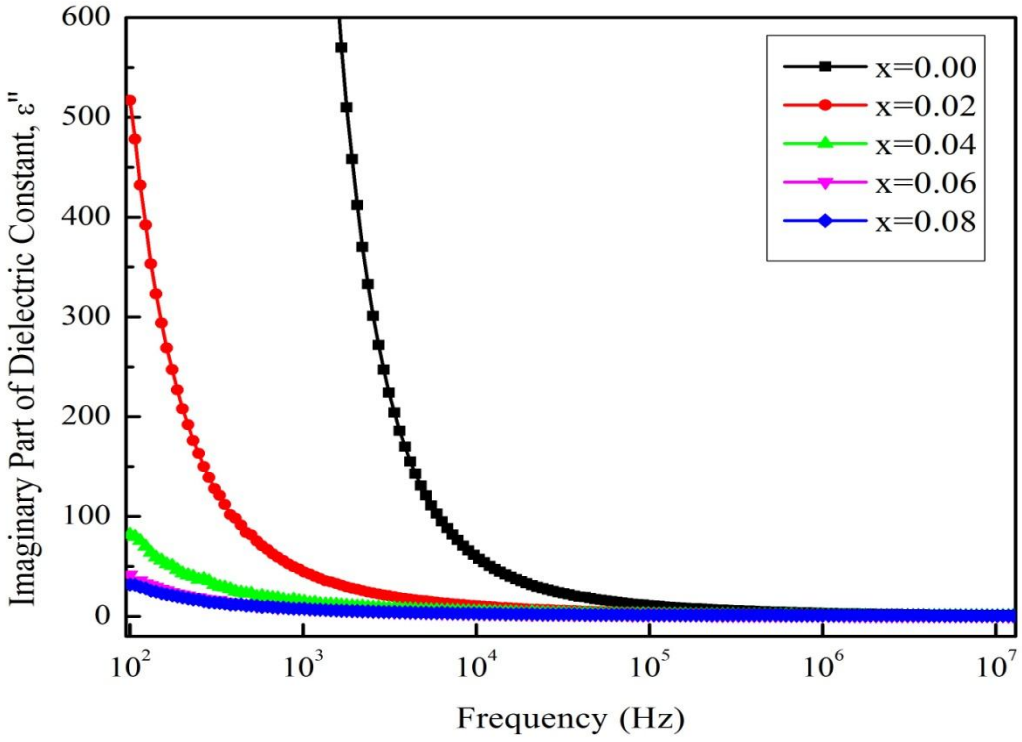

Figure 4.12: Frequency dependent imaginary part of dielectric constant of $Co_{0.25}Zn_{0.75}Yb_xFe_{2-x}O_4$, [Where x=0.00, 0.02, 0.04, 0.06 and 0.08] ferrites sintered at 1150°C for 3 hours

At low frequency the grain boundaries are more effective and at high frequency grains are effective [Ahmed *et al.*, 1989]. For this reason, grain boundary

effect is responsible for decreasing imaginary part of the dielectric constant rapidly at low frequency region. At high frequency the polarization decreased, thus resulting in a decrease in imaginary part of the dielectric constant.

Figure 4.13 shows the variation of $\tan\delta_E$ with frequency for ferrites at room temperature. The values of loss tangent decreases with increasing Yb content in $Co_{0.25}Zn_{0.75}Yb_xFe_{2-x}O_4$ ferrites. The variation of $\tan\delta_E$ with respect to frequency can be explained by two mechanisms: electron hopping and charge defect dipoles. The formation of dipoles contributes to loss tangent in the low frequency range and defect dipoles are responsible at high frequency range. We know that dipoles in ferrites are formed due to exchange Fe^{3+}- Fe^{2+} exchange, during sintering process. In the low frequency region ferrite contains high resistivity, then grain boundary requires more energy to exchange electron between Fe^{2+}-Fe^{3+} ions. For this reason the energy loss factor, $\tan\delta_E$ is high in the low frequency range. Similar behavior has been observed in the $\tan\delta_E$ vs frequency for ferrite composite by [Slatineanua *et al.*, 2013].

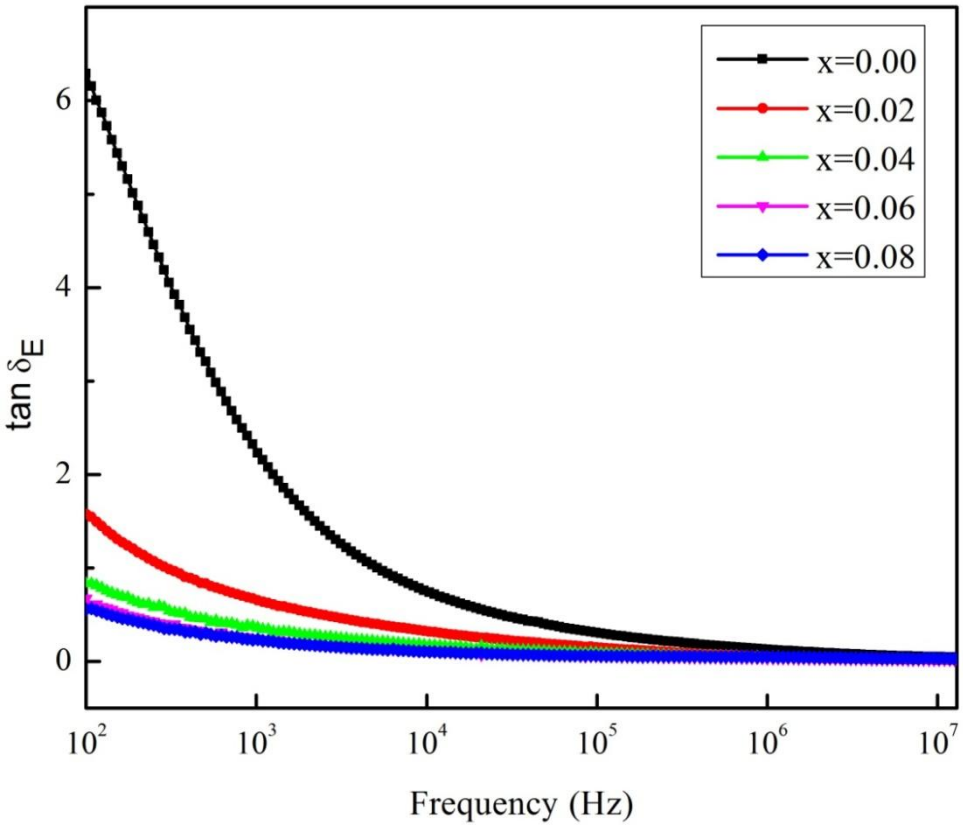

Figure 4.13: Frequency dependent dielectric loss of $Co_{0.25}Zn_{0.75}Yb_xFe_{2-x}O_4$, [Where x=0.00, 0.02, 0.04, 0.06 and 0.08] ferrites sintered at 1150°C/3 hours.

4.5 Effect of Ytterbium substitution on resistivity

Figure 4.14 shows the variation of DC resistivity as a function of Yb content in Co-Zn ferrites. From Figure 4.14 we can see that DC resistivity increases from to with increasing Yb content. We can explain this phenomenon by Verway's hopping mechanism. According to Verway's the electric conduction in ferrites is mainly due to hopping of electrons between ions of the same element present in more than one valance state, distributed randomly over the crystallographically equivalent lattice sites. In a spinel ferrite the distance between B-B sites is smaller than B-A sites so the electron hopping between B-A sites is smaller than B-B sites. Without Yb content(x=0.00), Fe concentration is maximum at B-site. When the Yb content increased in A-site, a decrease of Fe ion observed in B-site. Here some Fe ion migrated from A to B site to accommodate the increased number of Yb ions at A-sites. For this reason, electron hopping between Fe and Fe is greater at B-site. As Fe ion lowers the conduction and subsequently an increase in resistivity is observed.

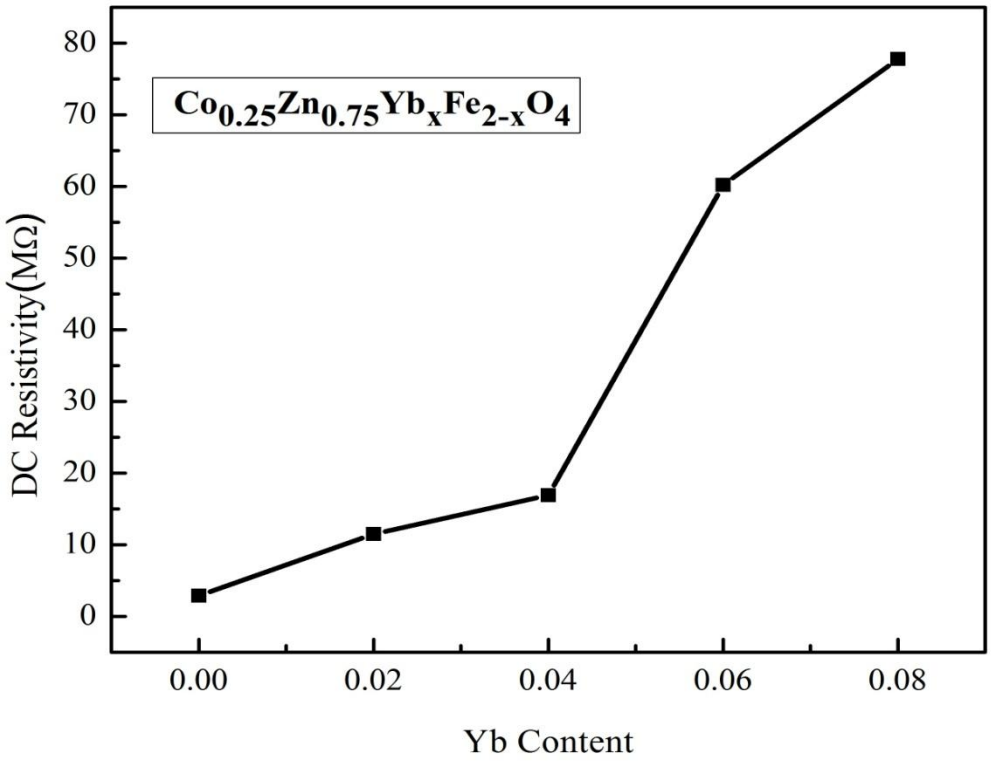

Figure 4.14: Variation of DC resistivity with Yb content

4.6 Finding the Optimum Value

Finding the optimum value of studied Co-Zn ferrite is a big challenge to us where both of ferroelectric and ferromagnetic orders contribute to the successful development of ferrite material. In this study we already mentioned about the electric and magnetic properties of $Co_{0.25}Zn_{0.75}Yb_xFe_{2-x}O_4$. Here, the dielectric properties were improved by adding Yb content. On the other hand, Yb doped Co-Zn ferrite shows weak ferromagnetic properties. So, we need to find the optimum useful parameters with combining electric and magnetic properties. To obtain the optimum mass fraction of the composites, also cross checked the magnetic and electric properties of the composites. Table 4.6, demonstrates the different values of permeability, magnetic loss tangent, dielectric constant, and dielectric loss tangent of $Co_{0.25}Zn_{0.75}Yb_xFe_{2-x}O_4$ composites [Where x = 0.00, 0.02, 0.04, 0.06 and 0.08] sintered at 1150°C at 1KHz frequency.

Table 4.6: For 1KHz frequency the comparison between permeability, magnetic loss tangent, dielectric constant, dielectric loss tangent of $Co_{0.25}Zn_{0.75}Yb_xFe_{2-x}O_4$ composites [Where x=0.00, 0.02, 0.04, 0.06 and 0.08] sintered at 1150°C holding time 3 hours.

Content	Magnetic Permeability	Magnetic Loss Tangent	Dielectric Constant	Dielectric Loss Tangent
X = 0.00	14.87	20.63	576	2.23
X = 0.02	14.40	17.29	68	0.65
X = 0.04	13.95	17.13	41	0.36
X = 0.06	13.59	16.66	32	0.25
X = 0.08	12.92	16.08	32	0.23

Figure 4.15 represents the variation of Dielectric constant and magnetic permeability of $Co_{0.25}Zn_{0.75}Yb_xFe_{2-x}O_4$ composites. It is observed that that for x = 0.00 to 0.02 both of permeability and dielectric constant are optimized. From Figure 4.15 it is observed that both the dielectric and magnetic loss tangent have become minimum for the mass fraction of x = 0.08. Moreover from Figure 4.16, the composite for x = 0.02 is better for magnetic properties. On the other hand for mass fraction x = 0.8 the composite shows the most magneto electric coupling.

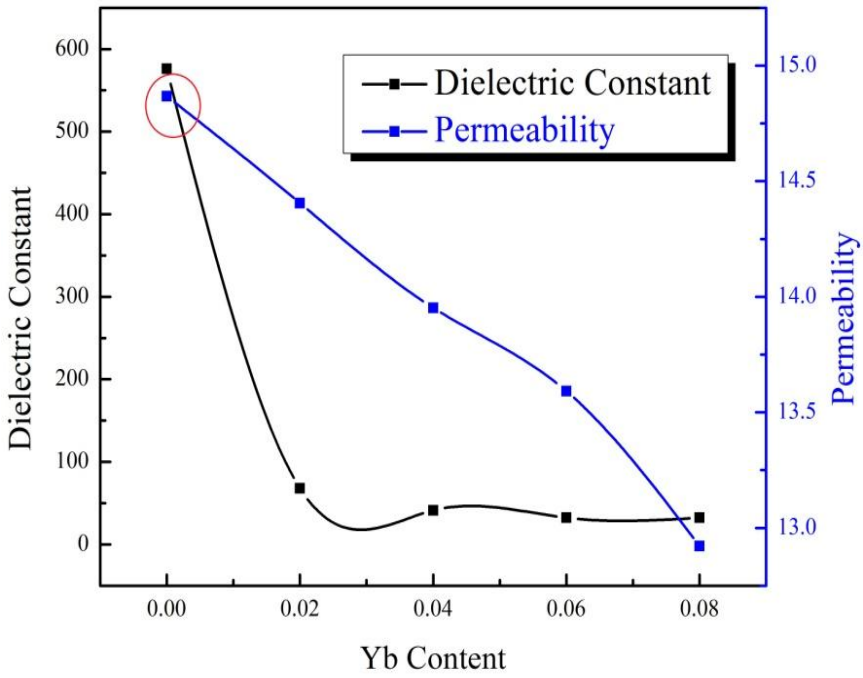

Figure 4.15: Comparison between Dielectric constant and Magnetic permeability of $Co_{0.25}Zn_{0.75}Yb_xFe_{2-x}O_{4,}$ composites with x=0.00, 0.02, 0.04, 0.06 and 0.08 sintered at 1150°C/3hrs.

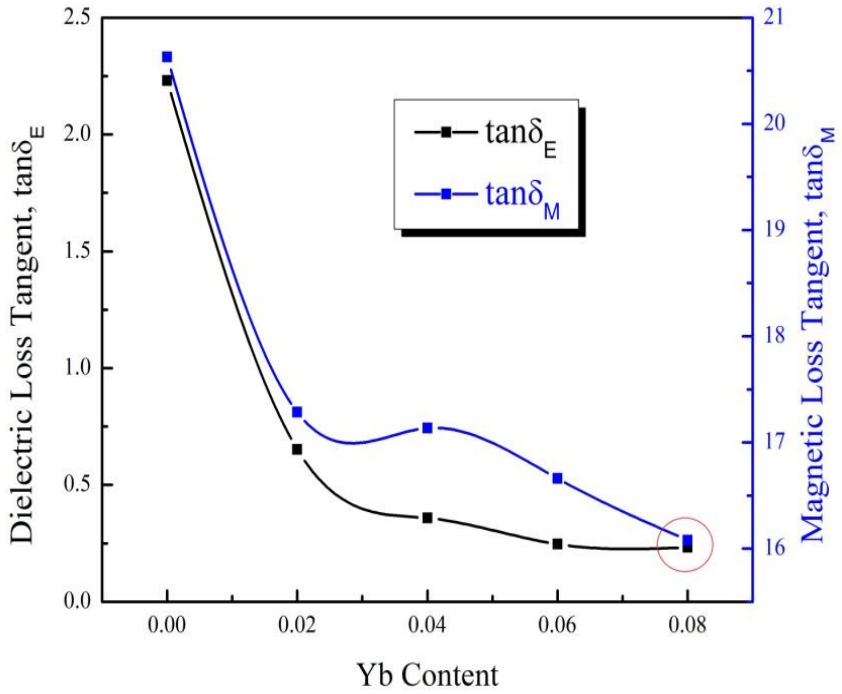

Figure 4.16: Comparison between Dielectric and Magnetic loss tangent of $Co_{0.25}Zn_{0.75}Yb_xFe_{2-x}O_{4,}$ composites with x=0.00, 0.02, 0.04, 0.06 and 0.08 sintered at 1150°C/3hrs.

CHAPTER V

CONCLUSIONS

CONCLUSIONS

5.1 Conclusions

The polycrystalline $Co_{0.25}Zn_{0.75}Yb_xFe_{2-x}O_4$ [Where x=0.00, 0.02, 0.04, 0.06 and 0.08] are successfully made by the standard solid state reaction method. The powder samples were annealed at 850°C and pallet and ring shaped samples were sintered at 1150°C. Powdered samples had used in XRD, pallet were used for dielectric measurement, resistivity measurement and SEM analysis. Ring shaped sample were used for permeability and magnetization measurements.

(i) The XRD patterns confirm that all the $Co_{0.25}Zn_{0.75}Yb_xFe_{2-x}O_4$ samples are of single phase cubic spinel structure without any impurity peaks.

(ii) Yb content having larger ionic radii (1.03Å) than the ionic radii of Fe (0.64Å). For this reason, the lattice parameter increases with the increase in Yb content, obeying the Vegard's law.

(iii) The bulk density is lower than the actual density of the sample. Bulk density is decreasing slowly with increasing Yb content. The porosity of the samples increases with increasing Yb content whereas porosity follows the opposite trend with bulk density.

(iv) SEM images showed that Yb^{3+} had a significant effect on the grain growth of the sample and the grain size slightly increased with increases Yb content. Average grain size is estimated in the range from 1.29μ to 2.35 μm.

(v) The magnetization measurement was carried out by VSM. Saturation magnetization decreases with increasing Yb content. Coercivity was increased with Yb content up to x = 0.06 after increase Yb content decreases. The values of Bohr magneton were found to be decreased with increasing Yb^{3+}content.

(vi) Frequency dependent initial permeability remains almost constant until very high frequency up to 50 MHz and then drops rapidly. The initial permeability is slightly decreases with increasing Yb content whereas magnetic losses in association with loss tangent decreased.

(vii) The frequency dependent imaginary permeability initially high at low frequency zone all the samples and then decreases with increasing frequency almost constant high frequency range. The grain growth increase with increasing Yb content diminishes the grain boundary.

(viii) The dielectric dispersion is rapid decreases at lower frequency region and it remains almost independent at high frequency side. The effect Yb^{3+} ion into Co-Zn ferrite has no pronounced effect of high frequency region but significantly decreases the dielectric constant in the low frequency region.

(ix) The rapid decrease of imaginary part of dielectric constant at lower frequency range is basis of space charge polarization. During the exchange process between Fe^{3+} to Fe^{2+} the electrons have to pass through the grains and grain boundaries.

(x) DC resistivity increases with increasing Yb content in Co-Zn ferrites. Basically Fe ion lowers the conduction and subsequently an increase in resistivity.

5.2 Scope for Future Work

Some studies on different aspects are possible for fundamental interest and also for potential applications of the studied materials. The following experiment and activities would be obtained as future work as the extension of this research.

- The characteristics in crystallization formation will be achieved by DSC thermal analysis.
- Neutron diffraction analysis may be performed for these compositions to determine the distribution of substituted ions between A and B sites. Mössbauer spectroscopy can also be studied.
- The bond length and bonding mechanism would be carried out by FTIR spectroscopy.
- Some AC and DC electrical properties may be studied.
- Temperature dependent magnetization and dielectric properties will be carried out to understand the effect of temperature.

REFERENCES

REFERENCE

Abbas M., Torati S. R., Rao B. P., Abdel-Hamed M. O. and Kim C. 2015: Size controlled sonochemical synthesis of highly crystalline superparamagnetic Mn-Zn ferrite nanoparticles in aqueous medium; J. Alloys Compd. 644, 774–782.

Ahmed M. A., Oskasha N. and Sayed M. M. EI. 2017: Enhancement of the physical properties of rare earth substituted Mn-Zn ferrites prepared by flash method; Ceramics International 33.1: 49-58.

Ahmed M. A., Ateia E., Salah Z. M., Gmal El. A. A. , 2005: Structural and Electrical Studies of La^{3+} substituted Ni-Zn ferrites; Mater. Chem. Phys. 92, 310.

Ahmed, M., El Nimr., M., Tawfik, A. and Aboel Ata, A. 1989: Dialectical Behavior in Co-Zn ferrites; Phys. Stat. Sol. (a), Vol. 114, pp. 377-382.

Akther Hossain A. K. M., Tabata H. and Kawai T. 2008: Magnetoresistive properties of $Zn_{1-x}Co_xFe_2O_4$ ferrites; J. Magn. Magn. Mater., 320: 1157-1162.

Alex Goldman 1990: Modern Ferrite Technology, Van Nosttrand Reinhold, New York, p-71.

Anshu Sharma, Kusum Parmar, Kotnala R. K. and Negi N. S. 2012: Magnetic and dielectric properties of $Co_xZn_{1-x}Fe_2O_4$ synthesized by metallo-organic decomposition technique; International Journal of Advances in Engineering & Technology 5.1: 544-554.

Bahadur D., Giri J. Nayak B. B., Sriharsha T., Prasad N. K. 2005: Processing, Properttyies and Some Novel Applications of Magnetic Nanoparticles; J. Pramana Phys. 65, 663.

Bharathi K. K., Chelvane J. A., Markandeyulu G.2009: Magnetoelectric properties of Gd and Nd-doped nickel ferrite; J. Magn. Magn. Mater. 321: 3677–3680.

Brailsford F. 1996: Physical Principles of Magnetism; D. Van Nostrand company Ltd., London.

Craik D. J. 1975: Magnetic Oxide; Part 1, John Wiley & Sons, Bristol, ch. 9, part-2.

Cullity B. D. 1972: Introduction to Magnetic Materials, Addison - Wisley Publishing Company, Inc.,California.

Dai H., Li T.; Xue R.; Chen Z. 2012: Effects of Europium Substitution on the Microstructure and electric Properties of Bismuth Ferrite Ceramics; J. Superconductor. Nov. Magn. 25: 109-1154.

Forner S. 1959: Versatile and sensitive Vibrating Sample Magnetometer; Rev. Sci. Instr. 30, P.548.

Globus A., Pascard H. and Cagan V. 1977: Distance between magnetic ions and fundamental properties in ferrites; Le Journal de Physique Colloques 38, C1-163

Goldman A. 1999: Handbook of Modern Ferromagnetic Materials; Kulwer Acad. Pub, Boston, U.S.A.

Gul I. H., Abbasi A. Z., Amin F., Anis-Ur-Rehman M. and Maqsood A. 2007: Structural, magnetic and electrical properties of $Co_{1-x}Zn_xFe_2O_4$ synthesized by co-precipitation method; J. Magn. Magn. Mater. 311: 494.

Guo L., Shen X., Meng X., Feng Y. 2010: Effect of Sm^{3+} ions doping on structure and magnetic properties of nanocrystalline $NiFe_2O_4$ fibers; J. Alloy. Compd. 490 : 301–306.

Gupta T. K. and Coble R. L. 1968: Sintering of ZnO: I, Densification and Grain Growth; J. Am. Ceram. Soe., 51, 521.

Hossain M. A., Khan M. N. I. and Sikder S. S. 2017: Structural Magnetic and Dielectric Behaviors of Y^{3+} Substituted Ni-Zn Ferrites; Int. J. of Nano Science Trends and Tech. 1.2: 1-19.

Hossain A. K. M. A. 1998: Investigation of colossal magnetoresistance in bulk and thick film magnetites; Ph. D. Thesis, Imperial College, London.

Jadhav S. R., Sawant S. S. and Patil S. A. 1999: Tempaerature and frequency dependence of initial permeability in Zr^{4+}substituted Cu-Zn ferrites; J. less-common Met., Vol. 158, pp.199 - 20.

Jacob B. P., Thankachan S., Xavier S., Mohammed E. M. 2011: Effect of Gd^{3+} doping on the structural and magnetic properties of nanocrystalline Ni–Cd mixed ferrite; Physica Scripta 84 : 045702.

Jacobo S. E., Uhalde S. D., Bertorello H. R. 2004: Rare Earth influence on the structural andmagnetic properties of Ni-Zn ferrites; *J. Magn. Magn. Mater.* **272:** 2253 - 2254.

Jie S., Lixi W., Naicen X., Qitu Z. 2010: Introduction to Ferrite; J. Rarte Earths, 28, 445.

Jing J., Liang-Chao L., Feng X. 2006: Preparation, Characterization and Magnetic Properties of PAN/La-substituted LINi Ferrite Nanocomposites; Chin. J. Chem., 24, 1804.

Jing J., Liang-Chao L., Feng X. 2007: Structural Analysis and Magnetic Properties of Gd-Doped Li-ni Ferrites Prepared Using Rheological Phase Reaction Method; J. Rare Earths 25, 79.

Ji-Jing Xu, Chun-Ming Yang, Hai-Feng Zou, Yan-Hua Song, Gui-Mei Gao, Bai-Chao An, Shu-Cai Gan 2009: Electromagnetic and microwave absorbing properties of Co_2Z-type hexaferrites doped with La^{3+}; Journal of Magnetism and Magnetic Materials 321: 3231–3235.

Jonker G. H. 1959: Analysis of the semiconducting properties of cobalt ferrite; J. Phys. Chem. Solids, 9(2), 165-175.

Kambale R. C., Song K. M., Koo Y. S. and Hur N. 2011: Low temperature synthesis of nanocrystalline Dy^{3+} doped cobalt ferrite: Structural and magnetic properties; J. Appl. Phys. 110: 053910.

Karimi Z., Mohammadifar Y., Shokrollahi H., Khameneh Asl Sh., Yousefi Gh., Karimi L. 2014: Magnetic and structural properties of nano sized Dy-doped cobalt ferrite synthesized by co-precipitation; Journal of Magnetism and Magnetic Materials 361: 150 –156.

Khan Z. H., Mahbubur Rahman M., Sikder S. S., Hakim M. A. and Saha D. K. 2013: Complex Permeability of Fe deficient Ni-Cu-Zn ferrites; Journal of Alloys and Compounds 548: 208-215.

Kittel C. 1996; Introduction to Solid State Physics; 7th edition, John Wiley & Sons, Inc., Singapore.

Kodama R. H. 1999: Magnetic nanoparticles; J. Magn. Magn. Mater. Vol. 200, pp. 359 - 372.

Kolekar C. B., Kamble P. N., Vaingankar A. S. 1995: Thermoelectric Power in Gd^{3+} substituted Cu-Cd Ferrites; J. Bull. Mater. Sci. 18(2), 133.

Laksman A., Rao K. H. and Mendiratta R. G. 2002: Magnetic Properties of In^{5+} and Cr^{3+} Substituted Mg-Mn Ferrites; J. Magn. Magn. Mater., Vol.250, pp.92 – 97.

Lijun Zhao , Hua Yang , Xueping Zhao , Lianxiang Yu , Yuming Cui , Shouhua Feng 2006: Magnetic properties of $CoFe_2O_4$ ferrite doped with rare earth ion; Materials Letters 60 : 1 – 6.

Lohar K. S., Pachpinde A. M., Langade M. M., Kadam R. H., Shirsath S. E. 2014: Selfpropagating high temperature synthesis, structural morphology and magnetic interactions in rare earth Ho^{3+} doped $CoFe_2O_4$ nanoparticles; J. Alloy. Compd. 604 : 204–210.

Lopez J., Gonzalez-Bahamon L. F., Prado J., Caicedo J. C., Zambrano G., Gomez M. E., Esteve J. and Prieto P. 2012: Study of magnetic and structural properties of ferrofluids based on cobalt-zinc ferrite nanoparticles; J. Magn. Magn. Mater. 324: 394.

Maxwell J. 1873: Electricity and Magnetism; Vol.1 Oxford University Press. London Wanger K. 1913: Ann. Phys. 40, 817.

Mendelson, M. I. 1969: Average Grain Size in Polycrystalline Ceramics; J. Am. Ceram, Soc. 52, 8,443 - 446.

Nakamura J., Miyamoto T. and Yamada Y. 2003: Complex Permeability Spectra of Polycrystalline Li-Zn Ferrite and Application of EM-Wave Absorber; J. Magn. Magn. Mater., Vol.256, pp.340 - 347.

Nalla Somaiah, Tanjore V. Jayaraman, Joy P. A., Dibakar Das 2012: Magnetic and magnetoelastic properties of Zn-doped Cobalt-ferrites $CoFe_{2-x}Zn_xO_4$ (x = 0, 0.1, 0.2, and 0.3); Journal of Magnetism and Magnetic Materials. 324: 2286-2291.

Nikumbh A. K., Pawar R. A., Nighot D. V., Gugale G. S., Sangale M. D., Khanvilkar M. B., Nagawade A.V. 2014: Structural, electrical, magnetic and dielectric properties of rare-earth substituted cobalt ferrites nanoparticles synthesized by the co-precipitation method; J. Magn. Magn. Mater. 355 : 201–209.

Nelson J. B., Riley D. P. 1945: An experimental investigation of extrapolation methods in the derivation of accurate unit-cell dimensions of crystals; Proc. Phys. Soc. London 57, 160.

Pandya P. B., Joshi H. H., Kulkarni R. G. 1991: Bulk magnetic properties of Co-Zn ferrites prepared by the co-precipitation method; Journal of materials science 26 : 5509-5512.

Peng J., Hojamberdiev M., Xu Y., Cao B., Wang J., Wu H. 2011: Hydrothermal synthesis and magnetic properties of gadolinium-doped $CoFe_2O_4$ nanoparticles; J. Magn. Magn. Mater. 323: 133–137.

Rahman M. T., Vargas M. and Ramana C.V. 2014: Structural characteristics, electrical conduction and dielectric properties of gadolinium substituted cobalt ferrite; J. Alloy. Compd. 617: 547–562.

Rare Earth Elements - Critical Resources for High Technology**:** United States Geological Survey, Fact Sheet 087-02.

Razia N., Khan S., Asokan K., Ahmed H. and Khan I. 2012: Magnetic and electrical properties of In doped cobalt ferrite nanoparticles; J. Appl. Phys. 112: 084321.

Rezlescu N., Rezlescu E., Pasnicu C., Craus M. L. 1994: Effect of the Rare Earth Metal of Some Properties of a Nickel-Zinc Ferrite; J. Phys Condensed Matter. 6 : 5707.

Standley K. J. 1972: Oxide Magnetic Materials; 2 ed., Oxford University Press.

Sajjia M., Oubaha M., Hasanuzzaman M.and Olabi A.G. 2014: Developments of cobalt ferrite nanoparticles prepared by the sol–gel process; Ceram. Int. 40: 1147–1154.

Shirsath S. E., Kadam R. H., Patange S. M., Mane M. L., Ghasemi A.and Morisako A. 2012: Enhanced magnetic properties of Dy^{3+} substituted Ni-Cu-Zn ferrite nanoparticles; Appl. Phys. Lett. 100: 042407.

Samokhvalov A. A. and Rustamov A. G. 1964: SOV. Phys. Solid State, 6, 749.

Sanpo and Noppakun: Solution Precursor Plasma Spray System, ISBN-9783319070247

Sathishkumar G., Venkataraju C. and Sivakumar K. 2010: Synthesis, structural and dielectric studies of nickel substituted cobalt-zinc ferrite; Materials Sciences and Applications. 1: 19–24.

Saroaut Noor 2011: Study of Additive Effects on the Structural, Magnetic and Transport properties of Cobalt Ferrites; Ph.D. Thesis, Khulna University of Engineering & Technology, Khulna.

Saroaut Noor, Hakim M. A., Sikder S. S., S. Manjura Hoque and Per Norddblad 2012: Magnetic behavior of Cd^{2+} substituted cobalt ferrites; Journal of Physics and Chemistry of Solids 73, pp.227-231.

Saroaut Noor, Sikder S. S. and Hakim M. A. 2010: Structural and Physics properties of Zn Substituted Cobalt Ferrites; Journal of Engineering Science (JES), Volume 1, Number2, pp.47-52.

Shil S. K., Sinha R. C., Hakim A. K. M. and Sikder S. S. 2012: Influence of Composition and Sintering Temperature on Magnetic and Electrical Properties of Spinel Type Ni –Zn Ferrite; Jahangirnagar University Journal of Science, Vol. 35, No. 2, pp. 23 – 36.

Shivaji R. Kulal, Sanjay S. Khetre, Pramod N. Jagdale, Vashishtha M. Gurame, Duryodhan P. Waghmode, Govind B. Kolekar, Sandip R. Sabale, Sambhaji R.

Bamane 2012: Synthesis of Dy doped Co–Zn ferrite by sol–gel auto combustion method and its characterization; Materials Letters 84 : 169 – 172.

Slatineanua T., Iordana A. R., Oanceaa V., Palamarua M. N., Dumitrub I., Constantinb C. P., Caltunb O. F. 2013: Magnetic and dielectric properties of Co–Zn ferrite; Materials Science and Engineering B. 13384: 1- 8.

Smit J. and Wijin H. P. J. 1959: Ferrites; Philips Technical Libery C Wiley, New York.

Sikder S. S.**,** Saroaut Noor, Hakim M. A., Per Nordblad and Saiduzzaman 2011; "Magnetization Behavior and Spin Canting in Diluted $Co_{1-x}Cd_xFe_2O_4$ Ferrites", AIP Conf. Proc. 1347, 310-313 doi:10.1063/1. 3601843@2011 American Institute of Physics 978-0-7354-0903-3/$30.00

Song J., Wang L., Xu N., Zhang Q. 2010: Microwave electromagnetic an absorbing properties of Dy^{3+} doped Mn-Zn ferrites; J. Rare Earths 28 : 451–455.

Tahir Abbas, Islam M. U. and Ashraf Ch M. 1995: Study of Sintering Behavior and Electrical Properties of Cu-Zn-Fe-O System; Mod. Phy. Letts., B 9(22), 1419.

Urcia-Romero S., Perales-Perez O. and Gutierrez G. 2010: Effect of Dy-doping on the structural and magnetic properties of Co–Zn ferrite nanocrystals for magnetocaloric applications; Journal Of Applied Physics. 107: 09A508.

Valenzuela R. 1994: Magnetic Ceramics; Cambridge University Press, Cambridge.

Vanuitert L. G.: High Resistivity Nickel Ferrites – the Effect of Minor Additions of Maganese or Cobalt; J. Chemi. Phys. 23, 1883.

Valenzuela R.1994: Magnetic Ceramics; Cambridge University Press., Cambridge.

Vegard's L. 1921: Die constitution der mischkristalle und die raumfullung der atome; Z. Phys. 5, 17.

Verway E. J. W. , Heilmann E. L. J. and Romeijin F. C. 1947: Physical Properties and Cation Arrangement of Oxides with Spinel Structure 11. Electronic Conductivity; J. Chem. Phys. 15 (4): 181 - 187.

Veverka M., Jirak Z., Kaman O., Knizek K., Marysko M., Pollert E., Zaveta K., Lancok A., Dlouha M. and Vratislav S. 2011: Distribution of cations in nanosize and bulk Co-Zn ferrite; Nanotechnology, 22: 345701.

Yan M. F. and Johnson D. W. 1978: Impurity induced exaggerated grain growth in Mn-Zn ferrites; J. Am. Ceram. Soc., **61**, 342.

Yang Z. H., Gong Z., Q., Li H. X., Ma Y. T. and Yang Y. F. 2006: Synthesis of Ni-Zn Ferrites and Its Microstructure and Magnetic Properties; Journal of Central South University of Technology, 13, 618-623.

Ying Zhang, Dijiang Wen 2012: Infrared emission properties of RE (RE = La, Ce, Pr, Nd, Sm, Eu, Gd, Tb, and Dy) and Mn co-doped $Co_{0.6}Zn_{0.4}Fe_2O_4$ ferrites; Materials Chemistry and Physics 131 : 575 – 580.

Zhang H. F., Or S. W., Chan H. L. W. 2008: Multiferroic properties of $Ni_{0.5}Zn_{0.5}Fe_2O_4$ - $Pb(Zr_{0.53}Ti_{0.47})O_3$ ceramic composites; J. Appl. Phys., 104:104109 –104114.

Zhenxing Yue, Zhou Ji, Longtu Li, Xiaolui Wang and Zhilun Gui 2001: Effect of copper on the electromagnetic properties of Mg-Zn-Cu ferrites prepared by Sol-gel auto-combustion method; Mater. Sci. Eng. B 86, 64.

CONFERENCE PUBLICATIONS

1. **M. D. Hossain**, M. A. Hossain, M. N. I. Khan and S. S. Sikder; "Study of Complex Permeability of Ytterbium Doped Co-Zn Ferrites", International Conference on Physics 2018, 08-10 March, DU, Dhaka-1000, Bangladesh.
2. **M. D. Hossain**, M. A. Hossain, M. N. I. Khan and S. S. Sikder; "Effect of the Yttrium (Y) Substitution on the Structural and Transport Properties in Co-Zn Ferrites"; Conference on Weather Forecasting and Advances in Physics, 11-12 May, 2018, KUET, Khulna-9203, Bangladesh.
3. **M. D. Hossain**, M. A. Hossain, M. N. I. Khan and S. S. Sikder; "Synthesis of Rare earth Yttrium substituted Co-Zn Ferrites and Study its Magnetic Properties", Conference on Weather Forecasting and Advances in Physics, 11-12 May, 2018, KUET, Khulna-9203, Bangladesh.